MAGNETIC AND MICROSTRUCTURE PROPERTIES OF IRON-RARE EARTH-CARBON MAGNETS

by

N. VENKATESWARAN

B.E., B.I.T.S. Pilani, India, 1985

A MASTER'S THESIS

submitted in partial fulfillment of the

requirements for the degree

MASTER OF SCIENCE

Department of Physics

College of Arts and Science

KANSAS STATE UNIVERSITY

Manhattan, Kansas

1988

Approved by:

George Hadjipanayis

Major Professor

A11208 306639

ND
2668
.T4
PHYS
1988
V46
c. 2

Acknowledgements

I am grateful to Dr.George Hadjipanayis for giving me the opportunity to work with him. Thanks are due to him for the support and encouragement through out this work. I would like to thank Dr M.J.O'shea and Dr.Talat Rahman for the useful discussions I had with them.

Thanks are due to Anton Nazareth, who helped me learn the intricacies of experimental methods in magnetism. It is also my pleasure to acknowledge the helpful assistance of all my teachers, colleagues and friends.

CONTENTS

page

ACKNOWLEDGEMENTS i
FIGURES iv
CHAPTER 1
Theoretical Background
1.1 Introduction 1
1.2 Domains 3
1.3 Anisotropy Energy 4
1.3.1 Domain walls and domain wall energy 5
1.4 Theories of coercivity 5
1.4.1 Domain wall pinning 5
1.4.2 Single domain particles 8
1.4.2(b) Coherent rotation of SDP 8
1.4.3 Nucleation of reversed domains 10
1.5 Permanent Magnets 11
CHAPTER 2
Previous Studies
2.1 Introduction to Fe-R-C systems 13
2.2 Objectives of present study 14
CHAPTER 3
Experimental Methods
3.1 Sample Preparation 15
3.2 Heat treatments 16
3.3 Magnetic measurements 16
3.4 TEM and X-ray observations 17
3.5 Samples studied 17
CHAPTER 4
Magnetic Measurements
4.1 Introduction 19
4.2 Initial curves and hysteresis loops 19
4.3 Temperature dependence of H_c 27
4.4 Thermomagnetic measurements $(M_H(T))$ 27
4.5 Ac susceptibility 32
CHAPTER 5
Microstructure
5.1 Introduction 37
5.2 Microstructure of $Fe_{77}Dy_{15}C_8$ 37
5.3 Microstructure of $Fe_{77}Nd_9Dy_6C_{7.2}B_{0.8}$ 38
5.4 Microstructure of $Fe_{76.1}Nd_{10.1}Dy_{5.9}C_{7.1}B_{0.8}$ 39
5.5 Microstructure of $Fe_{77}Nd_{15}B_8$ 40
CHAPTER 6

Analysis and Conclusions
6.1 Phase Diagram 53
6.2 Magnetic Hardening 54
6.3 Effect of C on coercivity 56
6.4 Effect of Nd on coercivity 56
6.5 Effect of Dy on coercivity 57
6.6 Conclusions 57
REFERENCES 60
ABSTRACT 63

Figures

1.1 Magnetization curve and hysteresis loop.
1.2 Model to illustrate domain wall movement.
1.3 The prolate ellipsoidal particle in a magnetic field.
1.4 Energy product and working point for a permanent magnet.
4.1 M Vs H curve for as cast $Fe_{77}Dy_{15}C_8$.
4.2 M Vs H curve for as cast $Fe_{77}Nd_9Dy_6C_{7.2}B_{0.8}$
4.3 M Vs H curve for as cast $Fe_{76.1}Nd_{10.1}Dy_{5.9}C_{7.1}B_{0.8}$
4.4 M Vs H curve for as cast H.T. $Fe_{77}Dy_{15}C_8$.
4.5 M Vs H curve for as cast H.T. $Fe_{77}Nd_9Dy_6C_{7.2}B_{0.8}$.
4.6 M Vs H curve for as cast H.T. $Fe_{76.1}Nd_{10.1}Dy_{5.9}C_{7.1}B_{0.8}$
4.7 Illustrating "ideal" domain wall pinning and "ideal" nucleation of reversed domains.
4.8 H_C Vs T for I, II, and III.
4.9 Magnetization Vs Temperature for I.
4.10 Magnetization Vs Temperature for II.
4.11 Magnetization Vs Temperature for III.
4.12 Ac susceptibility Vs Temperature for I.
4.13 Magnetization Vs Temperature (below RT) for I.
4.14 Magnetization Vs applied field for fine powders at T=300K.
4.15 Magnetization Vs applied field for fine powders at T=30K.
5.1 SEM of I showing three different grains.
5.2 Microstructure of a region of I.
5.3 Electron difraction pattern of region A in fig 5.2 showing the $Fe_{14}Dy_2C$ phase.
5.4 Lattice image of the 2:14:1 phase.
5.5 Microstructure of a different region of I.
5.6 Electron diffraction of region in fig 5.5.
5.7 SEM of II showing grains 1-2μm in size.
5.8 Microstructure of a faulted region of II.
5.9 Electron diffraction pattern of 2:14:1 phase showing distortion due to faults.
5.10 Lattice images seen in II.
5.11 Electron diffraction of fig 5.11 showing heaxagonal structure.
5.12 Microstructure of II showing oriented grains.
5.13 SEM of III.
5.14 domain walls(dw) in III.
5.15 2:17 phase corresponding to dw of fig 5.15.
5.16 Microstructure of some region of III.
5.17 2:14:1 phase corresponding to region X.
5.18 Lattice image of another region of III.
5.19 FeDyC phase corresponding to the lattice image of fig 5.18

5.20 SEM of as cast $Fe_{77}Nd_{15}B_8$.
5.21 SEM of as cast heat treated $Fe_{77}Nd_{15}B_8$

Chapter 1

THEORETICAL BACKGROUND

1.1 Introduction

A ferromagnetic material is one in which the strongly coupled atomic dipole moments tend to align parallel. As a result of this spontaneous magnetization exists in small domains in such materials; that is even in the absence of a magnetic field there is a net magnetic moment in the domains. Above a critical temperature, T_c called the ferromagnetic Curie temperature, the spontaneous magnetization vanishes. The material then becomes paramagnetic.

The principal bulk property of a ferromagnetic material is the appearance of a relatively large magnetization M with the application of a small field H, and the tendency of this magnetization to saturate at a value M_s in higher fields. Other properties used as a test for the occurrence of ferromagnetism are the existence of a "remanent magnetization" M_r after the removal of the applied field, and the existence of irreversibility or "hysteresis", in the M-H magnetization curve. A hysteresis loop is shown in Fig 1.1 . With reference to this Figure, H_c called the coercive field or "coercivity", is the magnetic field that must be applied in an opposite manner to "reduce" the magnetization M to zero.

Similar effects occur in the B-H magnetization curve, where B is the induction, or flux density defined as, [1],

$$B = H + 4\pi M \tag{1.1}$$

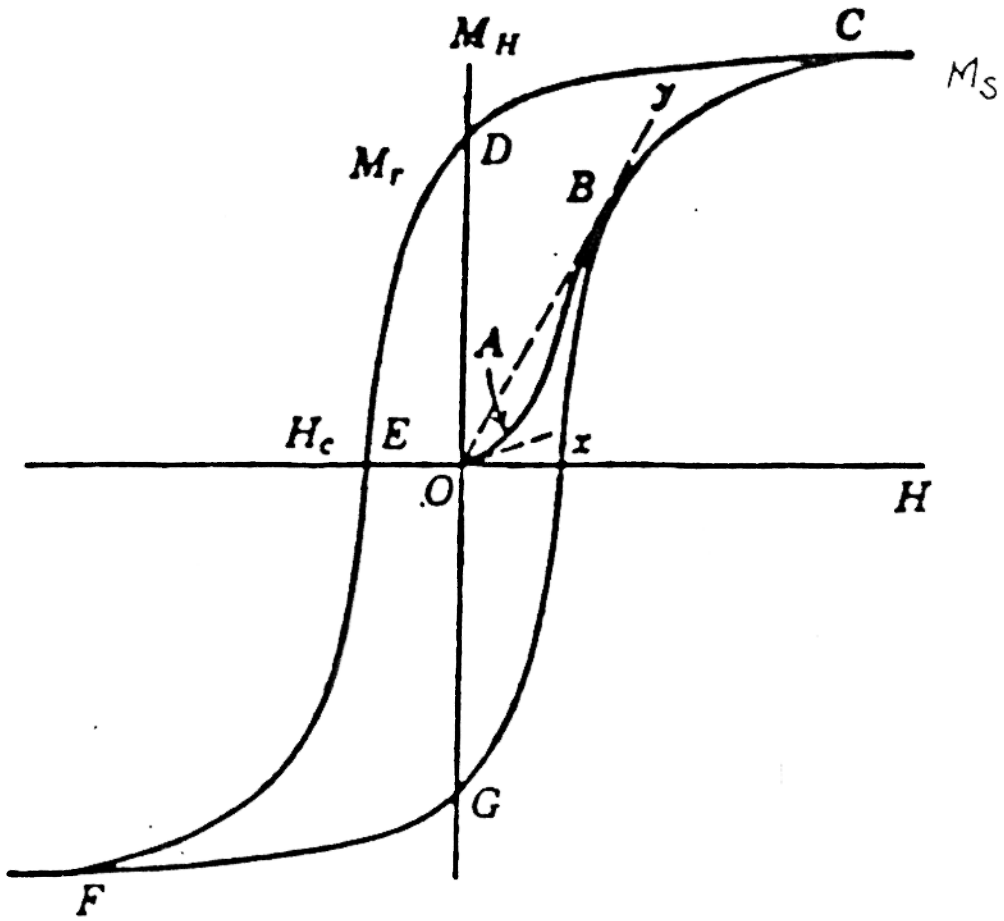

Fig 1.1 Magnetization curve (OABC) and hysteresis loop

(OCDEFGC) of a typical ferromagnetic material

The "residual induction" B_r is equal to $4\pi M_r$. In the cgs units used in this thesis, B is measured in gauss and H is measured in oersteds.

1.2 Domains

It is well known that in spite of the spontaneous magnetization a ferromagnetic specimen may exhibit no magnetic moment when the applied field is zero. In order to explain these observations, Weiss postulated the existence of small regions, called domains, each of which is spontaneously magnetized. The magnetization of the bulk material is then the vector sum of all the magnetizations present in the domains which make up the sample. Since the direction of magnetization in each domain need not be parallel, certain domain conFigurations lead to a zero net moment. The application of a relatively small field changes the domain arrangement, and hence leads to an appreciable net magnetization. The boundary region between two domains is called a domain wall, also called a Bloch wall.

The main reason for the existence of domains in a crystal is that their presence reduces the demagnetization energy associated with it. The true magnetic domain structure of a sample is found by minimizing the total energy.

The total free energy of a ferromagnetic specimen in an applied magnetic field may be written as the sum of several free energy terms [2]:

$$F_T = F_H + F_D + F_K + F_\sigma + F_\varepsilon + F_0 \tag{1.2}$$

where the symbols have the following meaning. F_T is the total free energy, F_H is the energy of the specimen's magnetization in the applied field H, F_D is the self

energy of magnetization in its own field, F_K is the crystalline anisotropy energy which comes from the fact that it is easier to magnetize a crystal in certain directions called "easy directions" than in others, F_σ is the magnetostrictive energy, F_e is the exchange free energy and F_0 represents any other contributions to the free energy that may be present.

1.3 Anisotropy Energy

Magnetic properties of a ferromagnet depend on the direction in which they are measured and therefore a sample possesses a certain magnetic anisotropy. There are several kinds of anisotropy : crystal anisotropy also called magnetocrystalline anisotropy, shape anisotropy, stress anisotropy etc. Only crystal anisotropy is intrinsic to the material. That is, all the others are external or can be induced in the material.

The preferred direction of magnetization of ferromagnetic materials are defined as "Easy Axes" . The crystalline anisotropy energy is defined as the work required to make the magnetization lie along a direction different from the easy direction. For a uniaxial crystal, the anisotropy energy is given by, [24],

$$E_k = K_1 sin^2\theta + K_2 sin^4\theta \tag{1.3}$$

where K_1 and K_2 are the anisotropy constants for a particular material.

1.3.1 Domain Walls and Domain Wall Energy

The change of magnetization through the boundary between magnetic domains is not abrupt but a gradual one, since the latter involves less exchange energy. For the simplest type, the 180° wall, the magnetization simply changes direction. The actual width of the wall is determined by the competition between F_e and F_K, assuming $F_D = 0$. It has been shown [2], that for a uniaxial crystal with 180° wall, the wall thickness is given by

$$\delta = \sqrt{\frac{J_e S^2 \pi^2}{K_1 a}} \tag{1.4}$$

where J_e is the exchange integral, K_1 is the anisotropy constant, and a is the ineratomic distance. The wall energy per unit area associated with this value of δ is, from (1.3) and (1.4),

$$\gamma = 2\pi\sqrt{\frac{J_e S^2 K_1}{a}} \tag{1.5}$$

1.4 Theories Of Coercivity

Any theory trying to explain coercivity is based on the irreversible movement of domain walls or irreversible rotation of the magnetization vector. Below we present some of the mechanisms by which coercivity is obtained.

1.4.1 Domain Wall Pinning

The hysteresis curve arises from irreversible energy changes. The simple model developed below will show how the various parts of the hysteresis curve may be

related to domain wall movements. Let us consider a 180° wall that lies parallel to the y, z plane and moves in the x direction when a field is applied, as in Fig 1.2. Let F_{wt} denote the energy arising from a unit area of one wall located at a certain position, regardless of the origin of this energy. Now suppose F_{wt} for this wall depends on x in the manner shown in Fig 1.2(b). When the field is zero, the wall will lie at an energy minimum, assumed to be at $x = 0$. When the field is applied the equilibrium position of the wall is given by

$$2MH = \frac{dF_{wt}}{dx} \tag{1.6}$$

Hence the action of the field will be to displace the wall to the right by an amount depending on the slope of the F_{wt} versus x curve. For positions on the wall between O and A in Fig 1.2(c) the motion is reversible. Once the wall has reached A it will spontaneously move to E. This motion is irreversible, since on decreasing the field the wall moves back to D and then to C , on reversing the field direction. Further increasing the field to the range EF the motion remains reversible and at F spontaneous motion occurs.

The coercive force is a measure of the field required to move a wall past energy barriers and therefore depends on the maximum value of $\frac{dF_{wt}}{dx}$. The remanence is the result of a wall being taken from one one energy minimum to the other by the application and subsequent removal of the field. An actual material will have many walls and the behaviour of the material may be found by superimposing the effects due to each wall or by taking the average situation for one wall.

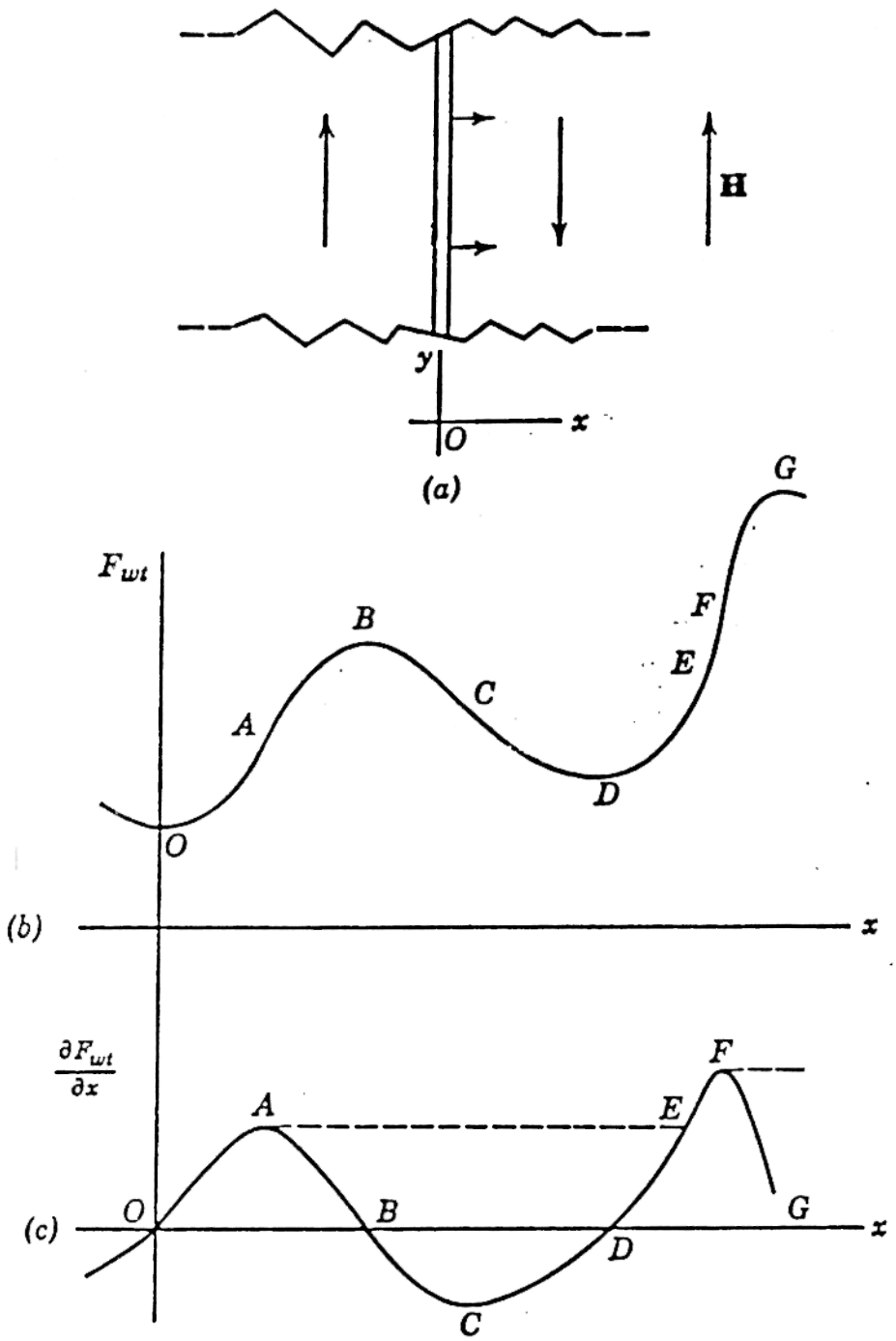

Fig 1.2 Model to illustrate domain wall movement, from Morrish [2]

In short, the theory of domain wall pinning predicts that imperfections or inclusions, magnetic or otherwise, impede domain wall motion and **increase** the coercivity. From equation (1.6) we get

$$H = H_c = \frac{(\frac{dF_{wi}}{dx})_{max}}{2M_s} \tag{1.7}$$

where the symbo ls have their usual meaning. The coercive force is a measure of the field required to move a wall past the energy barriers and therefore depends on the maximum value of $(\frac{dF_{wi}}{dx})$.

1.4.2 Single Domain Particles

A magnetic sample spontaneously breaks up into a number of domains in order to reduce its magnetostatic energy. But under certain circumstances the sample may remain a single domain. This happens when the sample is a very small particle. Then the exchange forces dominate, so that inspite of the presence of demagnetization energy, and the absence of an applied field the particle is uniformly magnetized and hence remains a single domain. The critical size for a sample to remain a single domain is given, by [24], as

$$L_c = \frac{1.7\gamma}{\pi^2 M_s^2} \tag{1.8}$$

1.4.2(b) Coherent Rotation of Single Domain Particles [2]

Consider a prolate ellipsoidal particle with F_k and F_σ equal to zero, and suppose a magnetic field is applied. At equilibrium, M will lie in the plane defined

by the directions of the field and the polar axis, as shown in Fig 1.3. The applied field, H, makes an angle θ with the polar axis.

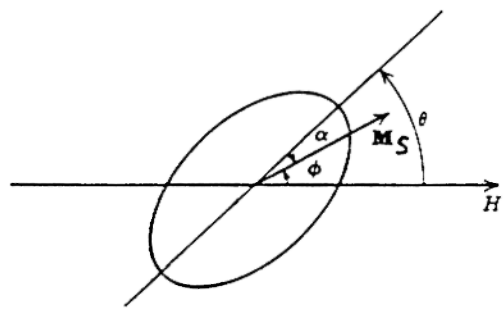

Fig 1.3 The prolate ellipsoidal particle

in a magnetic field, Morrish [2]

Now the demagnetization energy is given by

$$F_D = \frac{1}{2}M_s^2(D_a cos^2\alpha + D_b sin^2\alpha)V \tag{1.9}$$

where V is the volume of the particle and D_a, D_b are the demagnetization factors along the "a" and the "b" axis, respectively. The energy in the applied field is given by

$$F_H = -HM_sV cos\phi$$

where ϕ is the angle between H and M. Hence the total energy, from (1.2), is given by

$$F_T = constant - \frac{1}{4}(D_b - D_a)M_s^2 V cos2\alpha - HM_sV cos\phi$$

For equilibrium F_T must be minimized, and this will give the direction along which the particle will be magnetized. Minimizing F_T, and simplifying, we obtain

$$\frac{1}{2}sin2(\phi - \theta) + hsin\phi = 0 \tag{1.10}$$

where we define

$$h = \frac{H}{(D_b - D_a)M}$$

Now if we consider a particle with uniaxial anisotropy, instead of the shape anisotropy discussed above, neglecting K_2 and higher orders of K, and considering F_K instead of F_D in the expression for F_T, and minimizing it we get (1.10). But now h, the field in reduced units, is given by

$$h = \frac{HM_s}{2K_1}$$

Hence the maximum coercive force occurs for h = 1, that is $H = \frac{2K_1}{M_s}$. For a powder of spherical non interacting particles oriented randomly, $H_c = \frac{0.64K_1}{M_s}$, [2].

1.4.3 Nucleation Of Reversed Domains

This model was proposed to take care of the large discrepancies between observed and theoretical coercivities predicted by single domain particles . Brown [4] showed that the field required to reverse the magnetization in a perfect crystal is given by

$$H_c = \frac{2K}{M_s} \tag{1.11}$$

However, the coercivities in actual crystals are much less. The condition for wall nucleation, which means the generation of one or more nuclei possessing a reversed magnetization, is [24]

$$H_a + H_d > \frac{2K}{M_s} \tag{1.12}$$

where H_a is the applied magnetic field and H_d is the demagnetization field at the nucleation position. The applied field may be much less than expected if : 1)H_d or M_s is larger than normal or 2) K is smaller than normal. The value of M_s is determined by the magnetic moment per atom and the exchange coupling among atoms, and it may larger or smaller, in the vicinity of vacancies, interstitials, dislocations etc. The local value of K, which depends on spin-orbit coupling, may change due to imperfections or small variations in chemical composition. But it is believed that local variations in H_d play the prominent role in the nucleation of reversed domains. To put it succinctly, in this theory inclusions tend to **decrease** the coercivity, by making magnetization reversal easy.

1.5 Permanent Magnets

On the basis of theories described earlier, we can classify magnetic materials as hard or soft depending on their intrinsic coercivities. Accordingly, a hard magnetic material is one which has an intrinsic coercivity of at least 100 Oe.

In order for a material to serve as a permanent magnet three things are necessary: a large value of remanence, a high coercivity, and a high value of T_c. The product of the magnetic flux density B and the associated opposing field H,

also is a useful measure for permanent magnet materials. The (BH) product is commonly referred to as the energy product. In Fig 1.4, the working point $(B_w H_w)$ has been so determined that the the (BH) product shows a maximum [5]. This is designated by the symbol $(BH)_{max}$. It is generally advantageous to have a large energy product, so that magnets can be made as small as possible. When $B_r = H_c$ the loop has a square form and the maximum energy product is given by [6]

$$(BH)_{max} = (\frac{B_r}{2})^2 \tag{1.13}$$

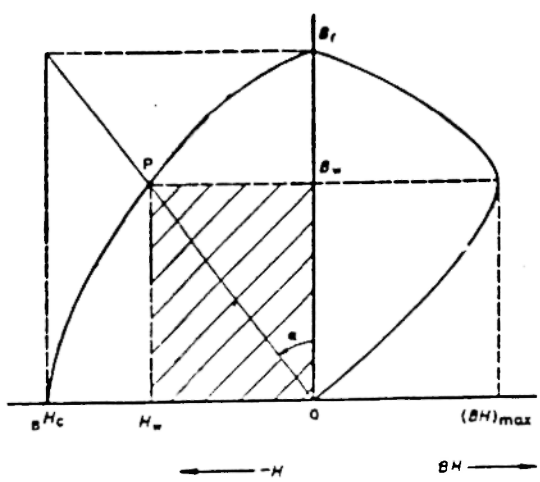

Fig 1.4 Energy product and working point for a permanent magnet, from Heck[5].

Chapter 2

PREVIOUS STUDIES

2.1 Introduction to Fe-R-C Systems [7-9]

Prior to 1980 the most popular permanent magnet materials contained samarium and cobalt. The critical and strategic importance of cobalt added to the short supply of samarium stimulated a lot of research in the development of new permanent magnets that would consist almost entirely of relatively cheaper, and more abundant, rare earths. In 1983,Hadjipanayis *et al* [10] reported the first non-cobalt FePrBSi magnet with a coercive field of 15 kOe and an energy product of 13 MGOe. Around the same time Croat [11] and Koon [12] reported similar results. As soon as these reports were released Sumitomo [13] announced the world's first iron-neodymium magnet (neomax) with a record energy product of 35 MGOe.

Since then, there has been a lot of activity, with the goal of understanding and improving the properties of the magnet systems prepared by sintering or rapid solidification techniques. The principal components of these systems remain Fe, Nd, and B ; minor additions to replace Fe or Nd serve chiefly to improve the high temperature behaviour of the Fe-Nd-B magnet. Using X-ray and neutron diffraction data , it has been determined [28]-[29] that the magnetic property of Fe-Nd-B is derived from the $Nd_2Fe_{14}B_1$, also called the 2:14:1 phase. The overall crystal structure of the 2:14:1 phase is tetragonal with a = 0.88 nm

and c = 1.22 nm, as shown in Fig 2.1 [14] . The fact that the tetragonal phase responsible for the high magnetic anisotropy is formed with carbon as the metalloid has largely been ignored even though such a compound was reported by Stadelmaier [15], two years before the disclosure of the Fe-R-B magnets. Stadelmaier reported the intermediate phases that are formed in the Fe-Gd-C alloy. The hard magnetic phase was reported to be $Fe_{20}Gd_3C$, now correctly identified as $Fe_{14}Gd_2C$. The Fe-Gd-C as-cast compound did not show the 2:14:1 phase but the heat-treated sample did. This led to a search for stable Fe-R-C, with R other than Gd, where it was supposed that these stable carbides would exhibit properties similar to Fe-Gd-C. Stadelmaier et Al [7-8], reported high coercivities in as-cast Fe-Dy-C alloys. However, they did not elaborate on the origin of these coercivities.

2.2 Objectives of Present Study

Our goal here, is to understand the mechanism by which a high coercivity is obtained in these carbides. In other words, is the high coercivity due to pinning, nucleation of reversed domains, or formation of single domain particles? We would also like to understand the exact role played by C, Dy in the achievement of high coercivities. To this end, we have conducted magnetic measurements as well as microstructure studies which gave us information about the structural morphology of the sample at different stages of heat treatment.

Chapter 3

EXPERIMENTAL METHODS

3.1 Sample Preparation

The samples obtained by melting together the constituents of the alloy is termed as an "as-cast" sample. As-cast samples of the alloys to be studied were made into buttons of 3-4 grams by arc-melting in high purity argon atmosphere. The purity of the materials was 99.9% or better for all elements used. The weight losses of the samples after melting were kept below 0.5%. The samples were remelted three times, so as to improve their homogeneity.

Powder samples were made by the following procedure: The as-cast samples were first ground into coarse powder by using a stainless steel grinding jar. This coarse powder was passed through a 100 mesh sieve and the coarse powders of around $150\mu m$ were obtained. Then the powder was ground into a finer size by ball milling. The time of milling was chosen to be around 24 hours so as to get single crystals of the sample. During the milling, the sample was always immersed in methylene chloride. For X-Ray studies the coarse powder was used.

Aligned powder samples were prepared by taking the powders and encasing them in a small piece of a plastic straw. Then the powders were aligned in a strong magnetic field and frozen in that conFiguration using molten wax. For TEM observations, the as-cast samples were first cut into a small slice using a

diamond cutter. Subsequently, these slices were shaped to a 3 mm diameter size discs by making use of the grinding wheel. These discs were then electropolished , and were then ready for TEM observation under the microscope.

3.2 Heat Treatments

The as-cast samples had to be heat-treated at 900°C for 72 hours.This high temperature required the use of quartz tubes.The samples were sealed inside the quartz tube that had been evacuated prior to this.For magnetic annealing,the samples in ceramic holders were heat-treated *in-situ* in a vibrating sample magnetometer,equipped with a furnace capable of temperatures upto 750°C and magnetic fields upto 17 kOe.Flowing argon gas served to protect the heated samples against oxidation.

3.3 Magnetic Measurements

Hysteresis loops were measured with a low field vsM (vibrating sample magnetometer) upto 17 kOe,and a high field vsM (upto 75 kOe).A range of temperatures from 4.2 K was provided by a Lakeshore temperature controller.A SQUID (superconducting quantum interference device) was used to provide additional data for temperatures ranging from 1.7 K to 400 K and for fields ranging upto 55 kOe. The high field vsM was used to measure M below room temperatures upto a maximum applied field of 75 kOe.

The temperature dependence of M, above room temperatures, was measured

to give us information about the different magnetic phases which are present in the sample and their transition temperatures. Such measurements are taken at very low applied fields, about 100 Oe, and the field is kept constant during the running of the experiment. The basic assumption of the method is that the total magnetization, $M_H(T)$ of a multiphase sample is a linear superposition of the magnetization of the individual phases.

Ac susceptibility (χ_{ac})measurements were also used to provide information about magnetic phase transitions. In this case the susceptibility of the sample is measured as a function of temperature in the presence of an alternating low applied field.

3.4 TEM and X-ray observations

Transmission electron microscopy (TEM) and electron diffraction, using a JEOL 100C scanning and transmission electron microscope,were used to examine the structure of the heat-treated and as-cast samples.A TEM can only give information about a small region of the sample.To get an overall picture of the structure X-ray measurements were made on the same samples.The d-spacings determined from the X-ray diffraction were matched with the known d-spacings of all possible phases in order to identify the phases present in the system. The X-ray diffraction studies were made using Cr (K_α) radiation.

3.5 Samples Studied

We basically dealt with four as-cast alloys having the following compositions:

(1) $Fe_{77}Dy_{15}C_8$

(2) $Fe_{77}Nd_9Dy_6C_{7.2}B_{0.8}$

(3) $Fe_{76.1}Nd_{10.1}Dy_{5.9}C_{7.1}B_{0.8}$

(4) $Fe_{77}Nd_{15}B_8$

For the sake of convenience, let us label the above compositions as I, II, III, and IV respectively. Samples I, II, and III were as-cast and heat-treated at 900℃ for approximately 72 hours. Sample IV was as-cast and heat treated at 900℃ for approximately 45 hours.

Chapter 4

MAGNETIC MEASUREMENTS

4.1 Introduction

In this chapter the magnetic properties of Fe-R-C-B alloys are discussed. The results are subdivided into sections that deal with different magnetic measurements. The objective of this work is to correlate the microstructure with the magnetic measurements and thus come up with a logical explanation for the large coercivity, observed experimentally, in these systems. The microstructure is presented in the next chapter.

4.2 Initial Curves and Hysteresis Loops

The initial magnetization curves and hysteresis loops were taken at room temperature. The as-cast (not heat treated) samples had negligible coercivities, Figs 4.1 - 4.3. Figs 4.4 - 4.6 show the hysteresis loops for the heat-treated samples. As it can be seen, the hysteresis loops showed a substantial increase in coercivity, after the samples were heat-treated. Therefore, most of our coercivity studies were focussed on samples which had been heat-treated.

The hysteresis loops do not appear to be saturated. Fig 4.4 shows an asymmetry about the Y axis and this is because the loops are minor loops. For all of the samples studied we observed a slight kink around around H = 0. This is most probably due to the presence of a soft magnetic phase[16], maybe α- Fe ?

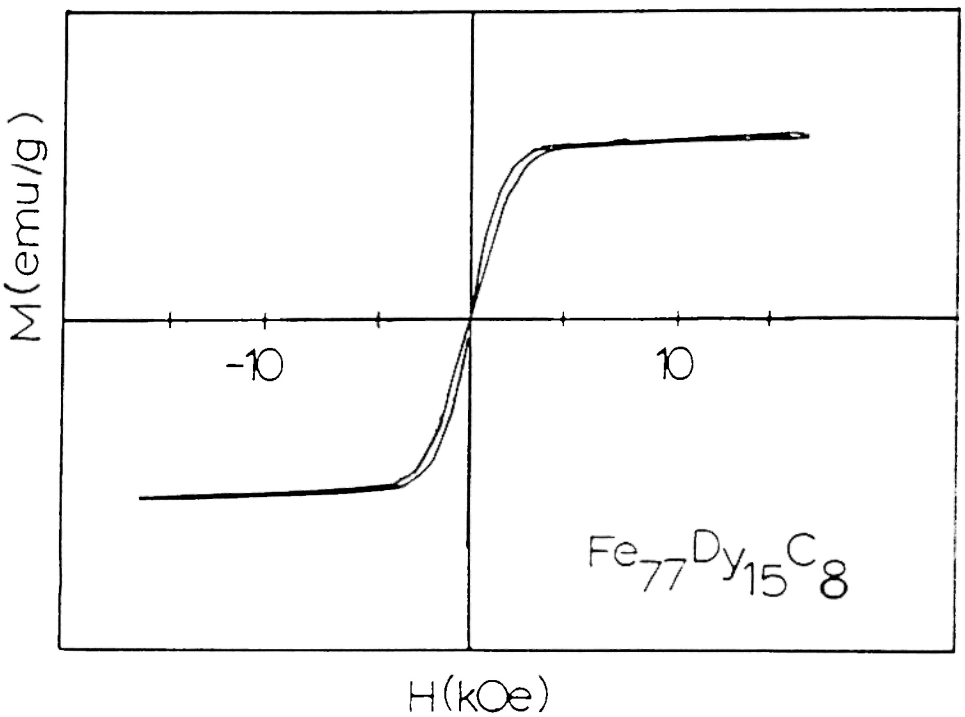

Fig 4.1 M vs H curve for as-cast $Fe_{77}Dy_{15}C_8$

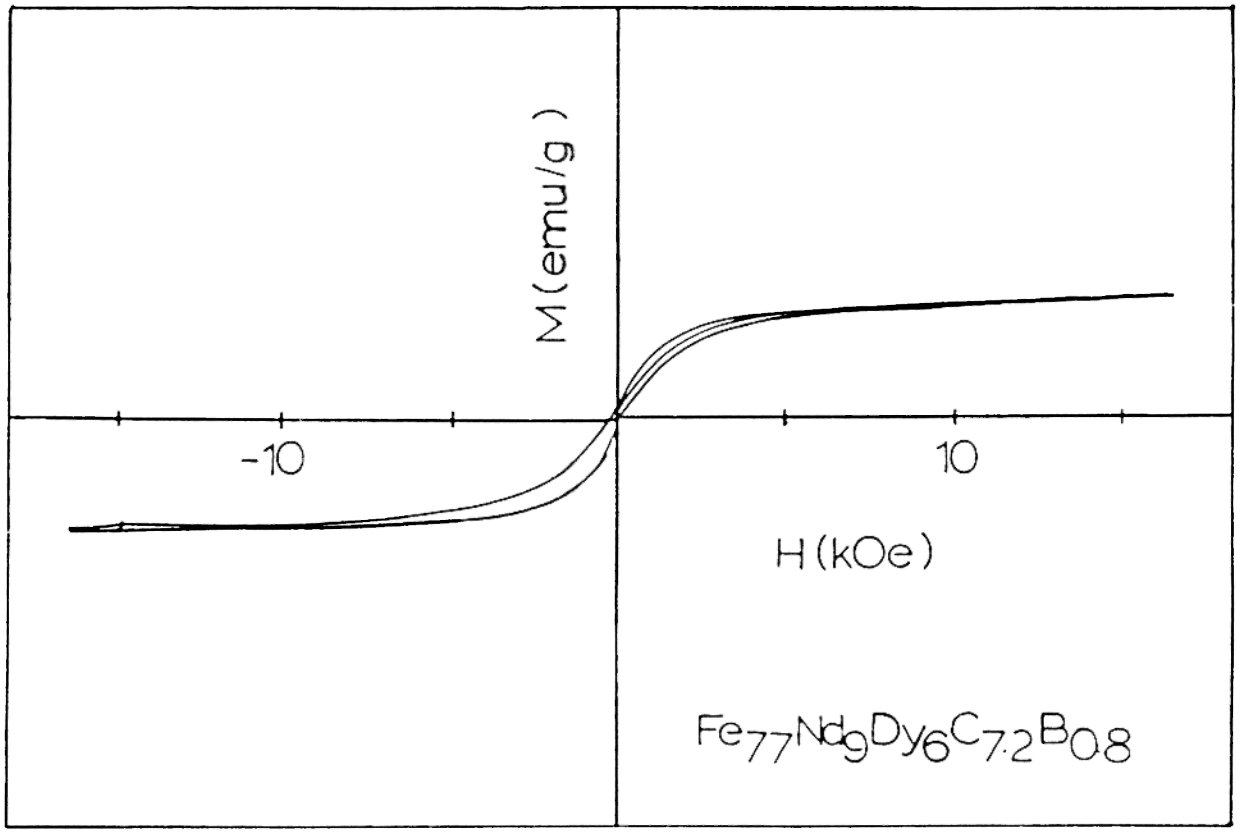

Fig 4.2 M vs H curve for as-cast $Fe_{77}Nd_9Dy_6C_{7.2}B_{0.8}$

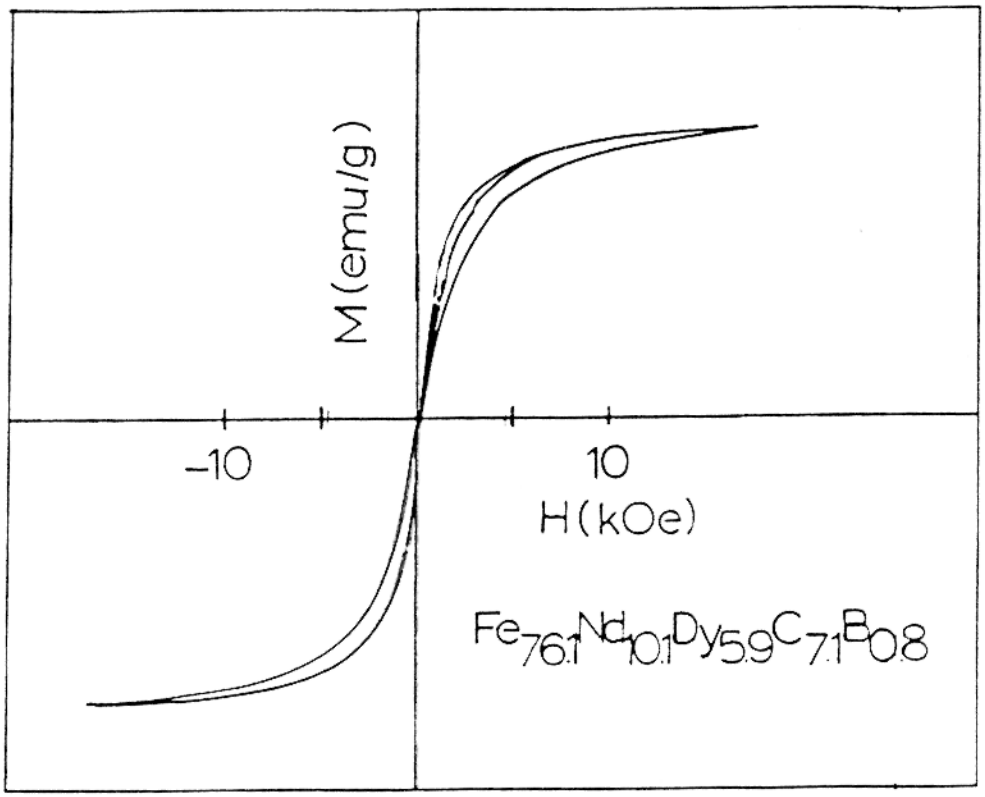

Fig 4.3 M vs H curve for as-cast $Fe_{(76.1)}Nd_{(10.1)}Dy_{5.9}C_{7.1}B_{0.8}$

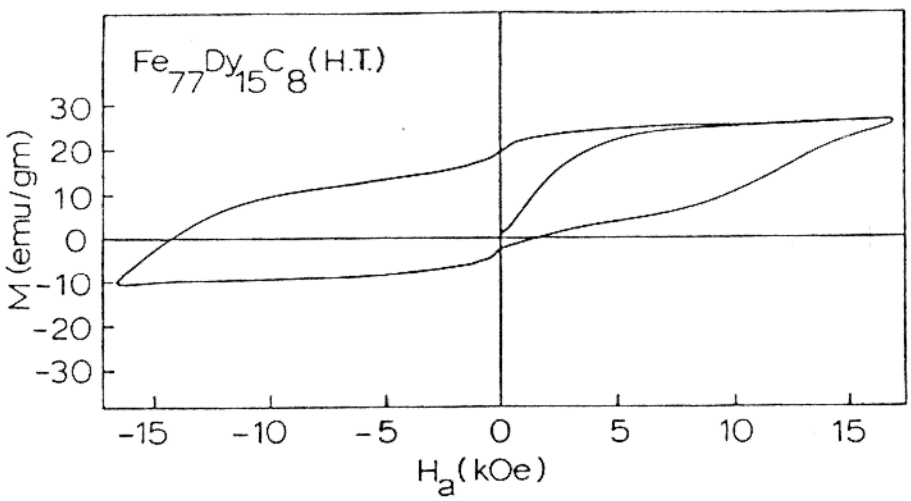

Fig 4.4 M Vs H curve for as cast H.T. $Fe_{77}Dy_{15}C_8$

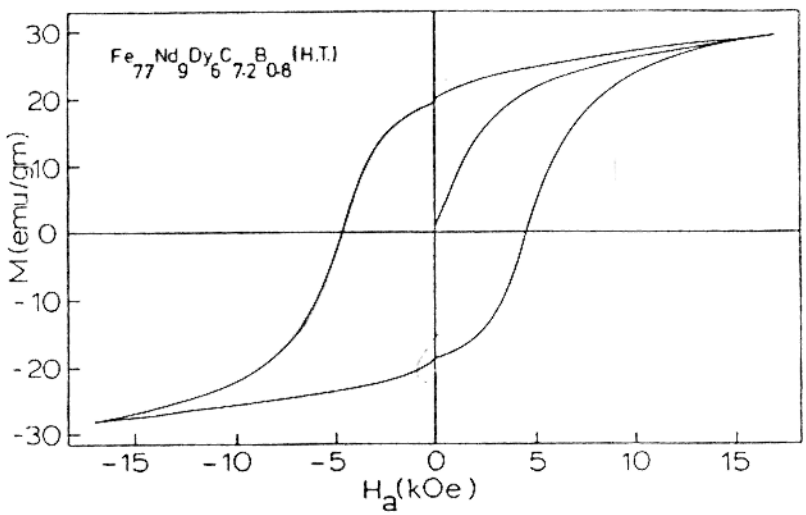

Fig 4.5 M Vs H curve for as cast H.T. $Fe_{77}Nd_9Dy_6C_{7.2}B_{0.8}$

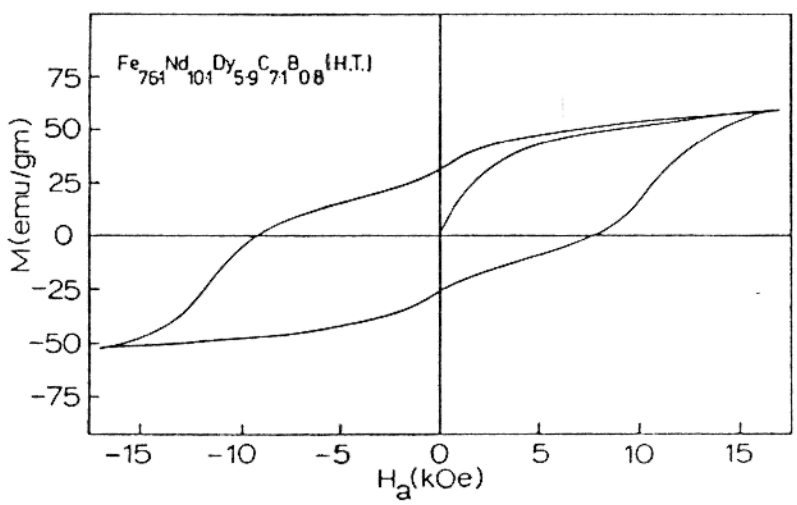

Fig 4.6 M Vs H curve for as cast H.T. $Fe_{76.1}Nd_{10.1}Dy_{5.9}C_{7.1}B_{0.8}$

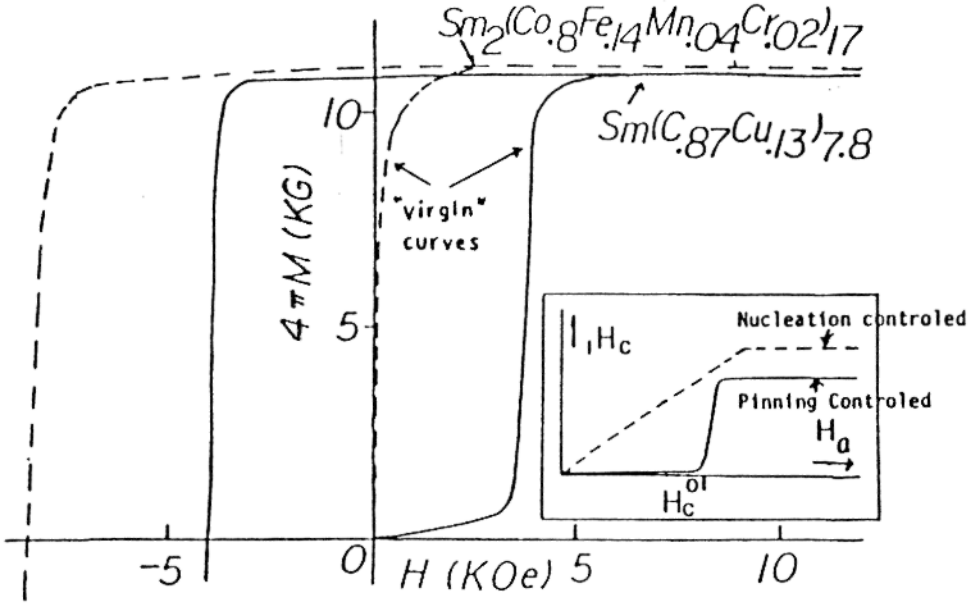

Fig 4.7 Illustrating "ideal" domain wall pinning

and "ideal" nucleation of reversed domains

The initial, also called "virgin", curves are very important in determining the coercivity mechanism. Figs 4.4 - 4.6 show the initial curves for the different samples. In all the three samples, for low values of H, M increases slowly and steadily for small increments of H and then it saturates at higher fields. For comparison purposes, Fig 4.7 shows the initial curves for two extreme situations: domain wall pinning and nucleation-type materials. It is obvious from Figs 4.4 - 4.7 that the initial curves of our samples are between the two extreme cases, although more closer to those of nucleation-type materials.

4.3 Temperature Dependence of H_c

Figs 4.8 shows the temperature dependence of H_c for I, II, and III respectively. Since the sample could not be saturated at fields of about 17 kOe, we used a high field of 75 kOe to check the temperature dependence of coercivity of I, for temperatures below 300 K. The coercivity, for I, shows a slight increase and then slowly tapers off to almost zero at around 300°C. For II and III the coercivity shows a slow decrease to zero.

The temperature coefficient of H_c is relatively small for the samples studied. This is in contrast to sintered Fe-Nd-B samples where the coercivity approaches zero at a much faster rate, at around 200°C [17]. As the temperature dependence of I, II, and III is similar, it strongly supports the idea that the coercivity mechanism in all three samples maybe the same.

4.4 Thermomagnetic Measurements ($M_H(T)$)

Figs 4.9 - 4.11 show the temperature dependence of M for the different samples, above room temperature. For I we observe a magnetic transition around 300°C, where the magnetization shows a sudden drop.For II and III we observe similar magnetic transitions at around 313 and 289 degrees Celsius. These temperatures correspond to the Curie temperature of the hard magnetic phase which is responsible for the magnetic properties observed in these samples. This hard magnetic phase could be the 2:14:1 phase since it has a curie temperature of about 300°C.Note that the magnetization does not go to zero at temperatures beyond 300°C. This is because of the presence of a small amount of $\alpha - Fe$. Table 4.1 summarises the magnetic properties of the above given samples.

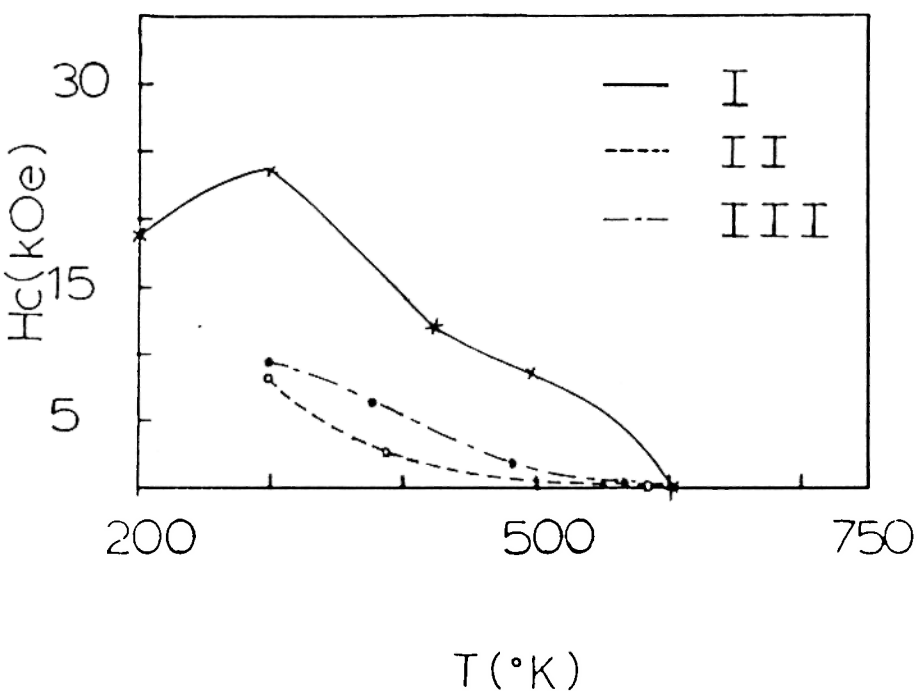

Fig. 4-8 Temperature dependence of H_c.

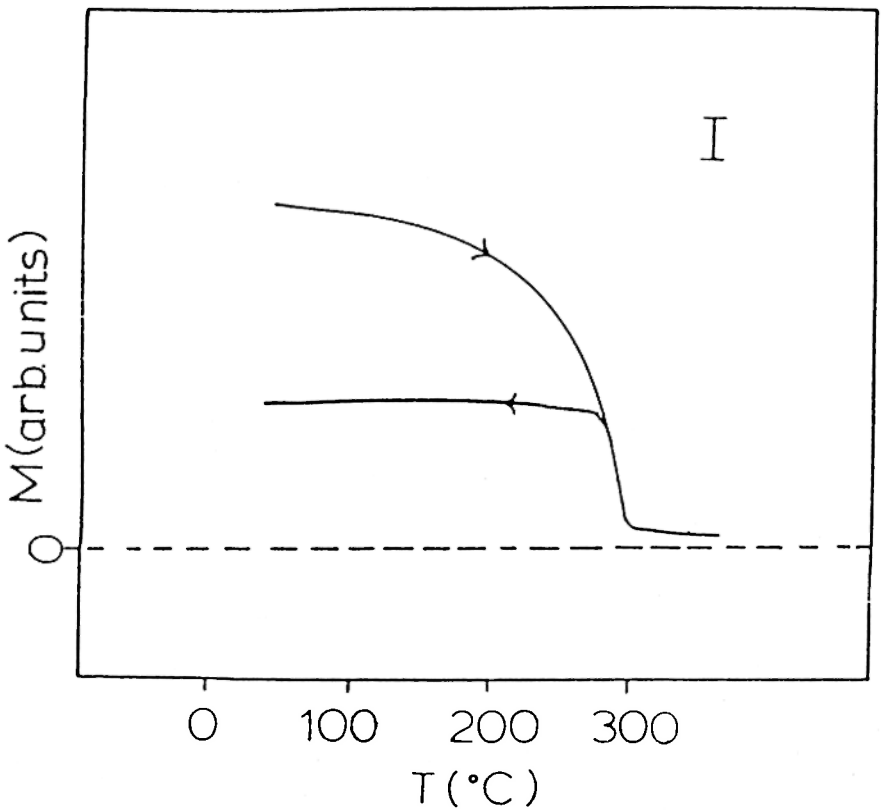

Fig 4.9 Magnetization vs Temperature for I

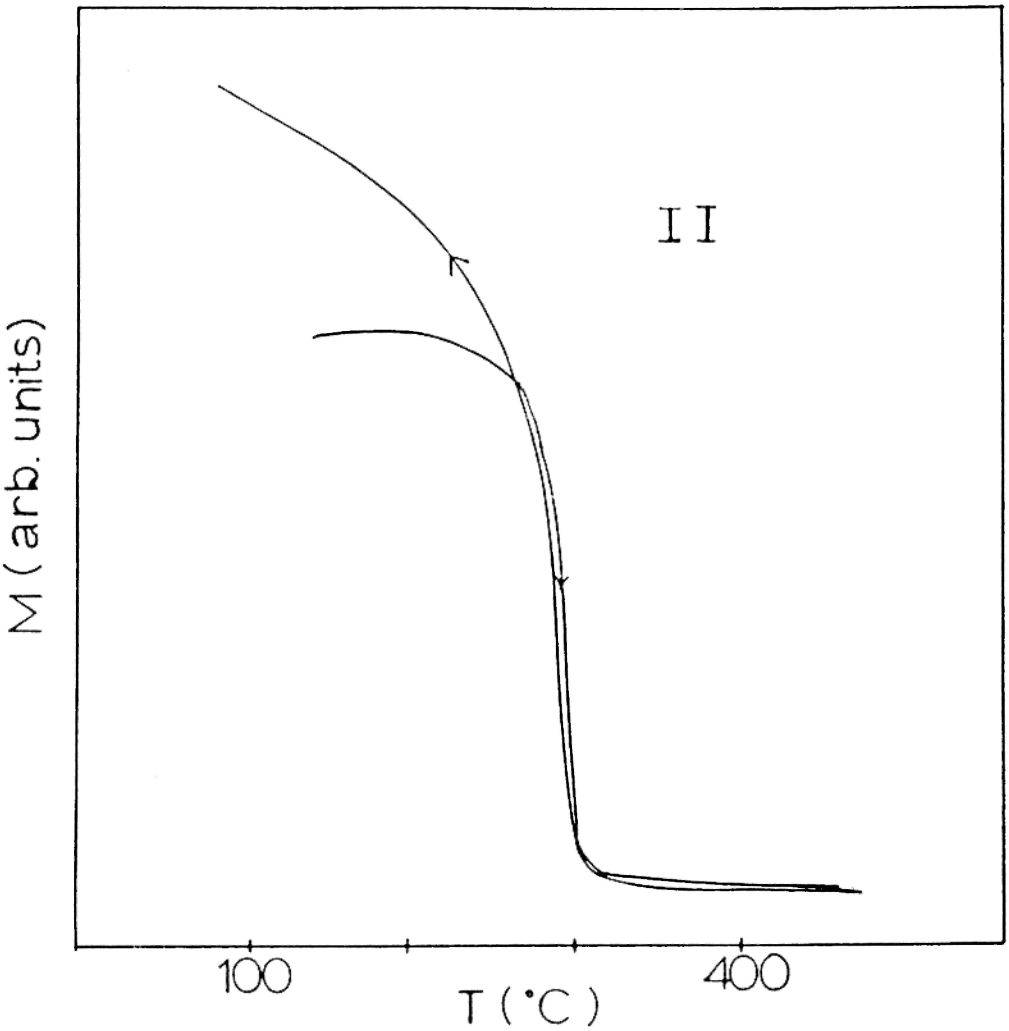

Fig 4.10 Magnetization Vs Temperature for II

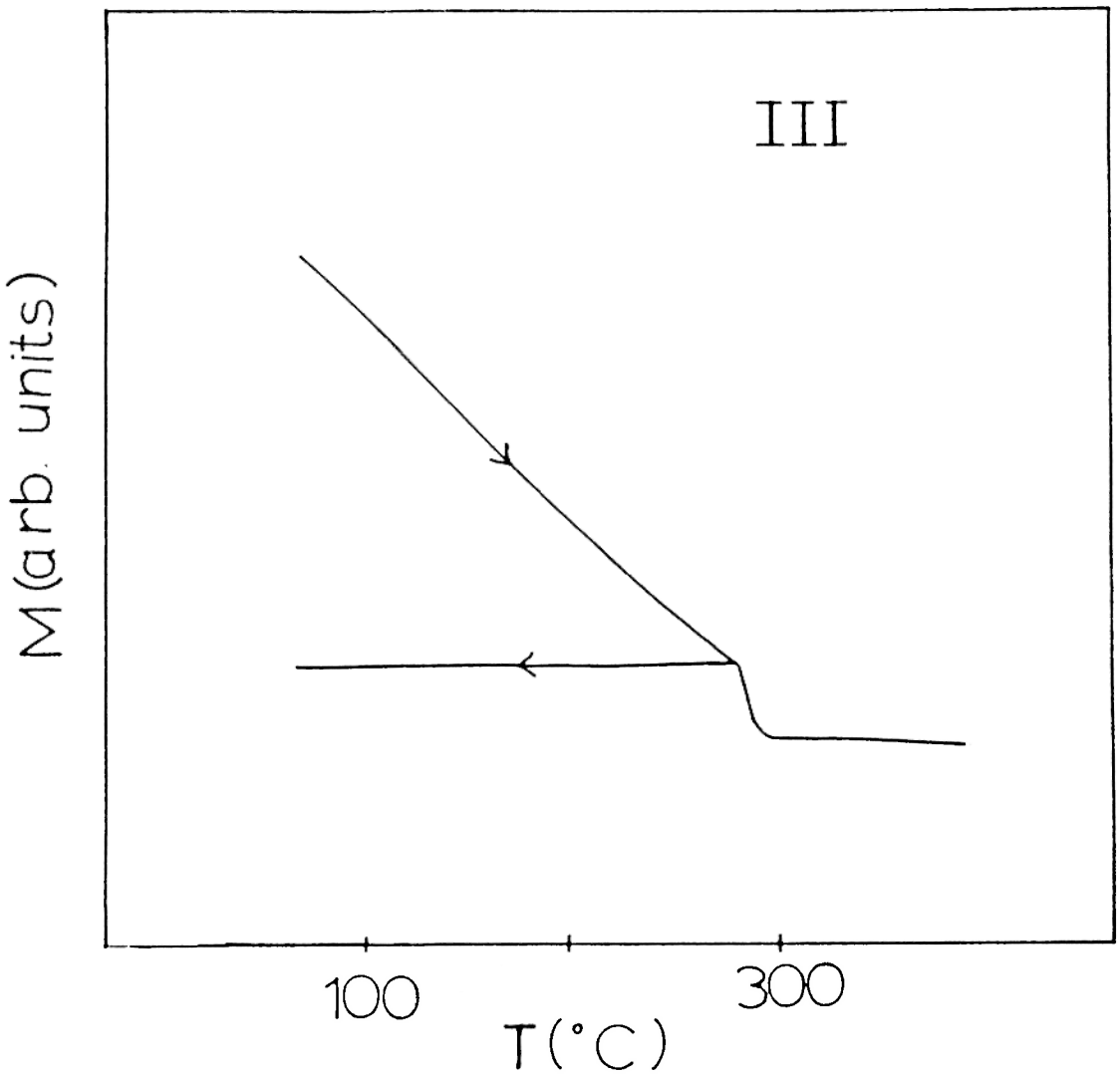

Fig 4.11 Magnetization Vs Temperature for III

4.5 AC Susceptibility

The susceptibility data for I is shown in Fig 4.12. We note that χ_{ac} shows a decrease as T is lowered. But at around 175 K an increase in χ_{ac} is seen. Note also the change in slope in Fig 4.13, which shows M (T) for I, with H = 50Oe. The anomalies observed in Figs 4.12-13 may be due to spin reorientation or due to the presence of a second phase. To answer this question we made fine powders and measurement M(H) for powders aligned parallel as well as for those aligned perpendicular to the applied field at T=300K and at T=30K . As can be seen, from Figs 4.14 - 4.15, at 300 K the set of data for parallel is consistently below the corresponding set of data for perpendicularly aligned powders. This is unlike the set of data taken at T=30K. So there seems to be some evidence for spin reorientation. A clearer picture can be obtained if a better method to prepare single crystals is used.

Table 4.1

sample	H_c	T_c	M_s^*
	(kOe)	($^\circ C$)	(emu/gm)
I	23	300	27.3
II	8.3	313	29.5
III	9.4	289	59.9
IV	-	310	44.54

* : M_s is the value of M obtained at 17 KOe.

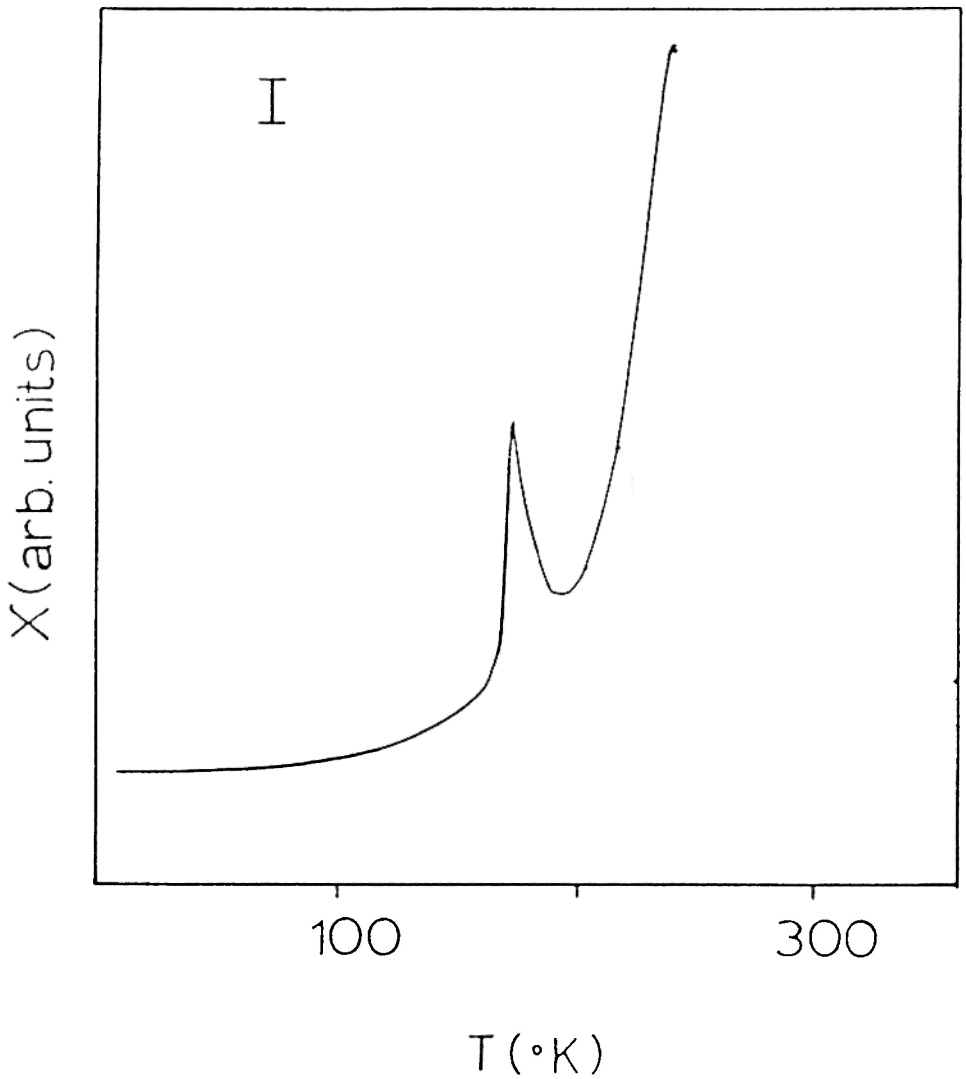

Fig 4.12 Ac suceptibility vs Temperature for I

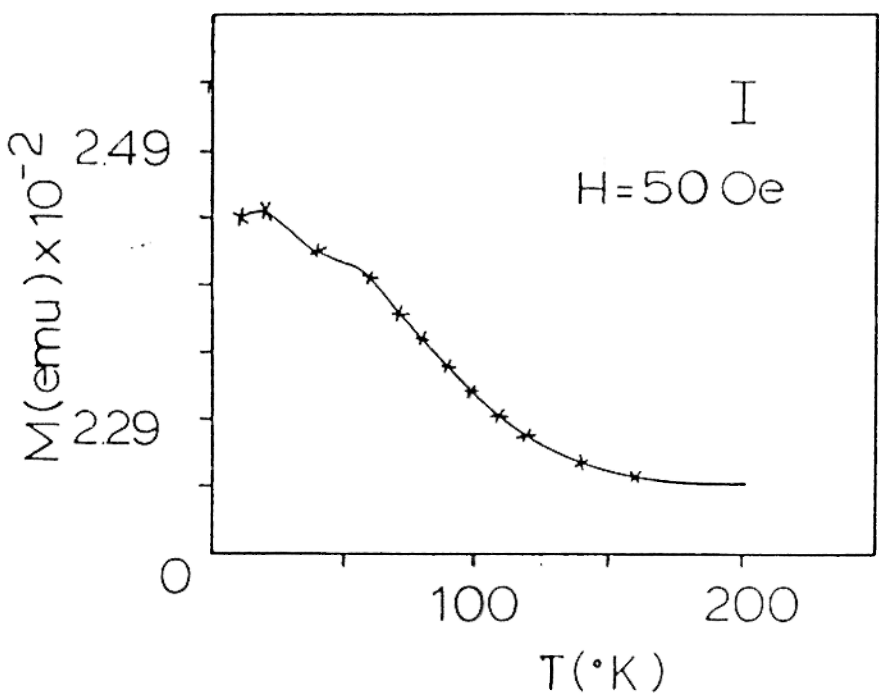

Fig 4.13 Magnetization vs Temperature (below RT) for I

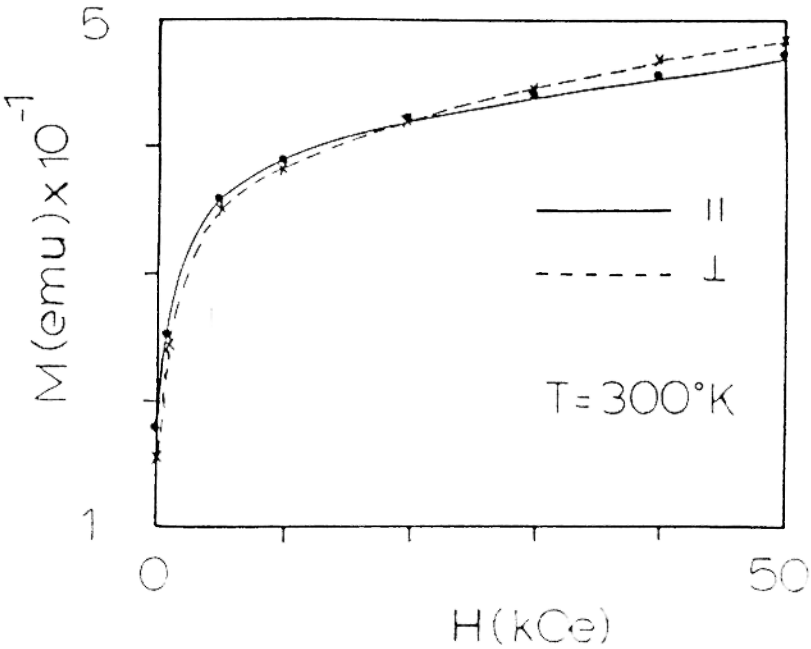

Fig 4.14 Magnetization vs Applied field for

fine powders of I at T=300K

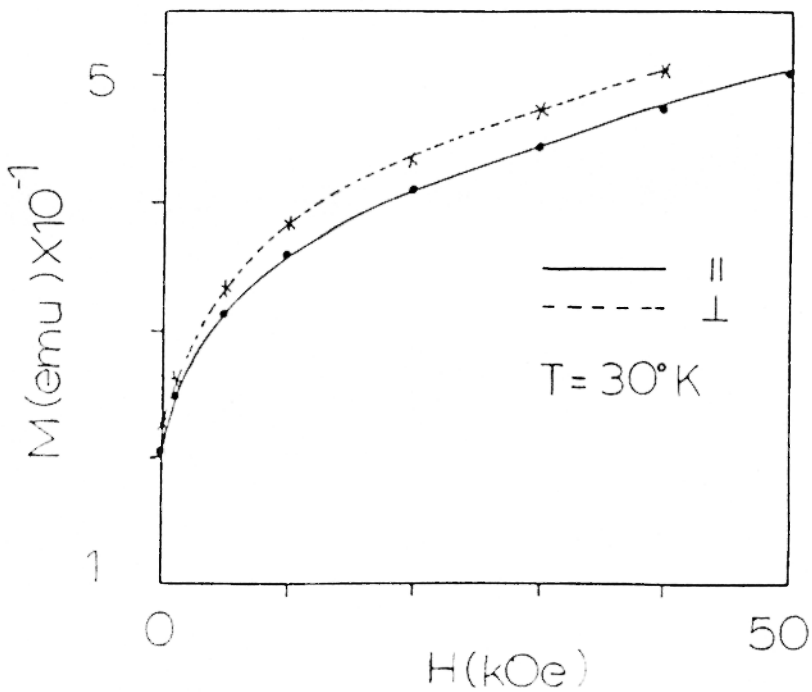

Fig 4.15 Magnetization vs Applied field for

fine powders of I at T=30K

Chapter 5

MICROSTRUCTURE

5.1 Introduction

The hard magnetic properties (H_c,M_R) of permanent magnet materials are dependent on their microstructure. Microstructure measurements are very important for the study and understanding of the origin of high coercivities. In this chapter we will present the microstructure of the samples studied.

5.2 Microstructure of $Fe_{77}Dy_{15}C_8$

SEM measurements were made to characterize the structure morphology and chemical composition of surface grains. Figs 5.1 shows three different grains, corresponding to a dark phase, a light phase and a white phase. The chemical composition of these regions was found by averaging a large number of data obtained through an energy dispersive X-ray analysis (EDXA). Unfortunately, EDXA cannot detect carbon or boron. So we have to make a guess about the final composition taking into account the TEM and metallurgical predictions. The results of EDXA showed that the light phase has 15 at% Dy and 85 at% Fe. This , most likely corresponds to the $Fe_{14}Dy_2C$ phase. The dark phase contains of about 25 at% Dy and 75 at% Fe and therefore is Dy richer. The white region has about 10 at% Dy and 90 at % Fe. This could possibly correspond to the $Fe_{17}Dy_2$ phase. Note that the white phase is very sparsely located. The grain

size is calculated to be approximately 6-10 μm.

The microstructure of a region of the sample obtained with TEM is shown in Fig 5.2 . Several grains are observed the smallest of which labelled G has a grain size of approximately $1\mu m$. It is difficult to estimate the size of the other grains, but they are probably bigger than $1\mu m$. The diffraction pattern from region A is shown in Fig 5.3, and has been identified to be the $Fe_{14}Dy_2C_1$, called 2:14:1 for convenience, phase. The indexing was done using a=8.756 A° and c=11.801 A°, [18]-[20]. Lattice imaging, Fig 5.4, shows a "d" spacing of approximately 1.18 nm. This agrees very well with the established c axis values for the 2:14:1 phase given earlier. Fig 5.5 shows the microstructure of a new region in sample I. The grainy region was selected for the diffraction pattern shown in Fig 5.6. The phase appears to be a mixture of the 2:14:1 , the Dy-rich and possibly, the Dy_2O_3 phases.

The phases determined from X-rays show the presence of the $Fe_{14}Dy_2C_1$ phase. This is consistent with the TEM pictures.

5.3 Microstructure of sample $Fe_{77}Nd_9Dy_6C_{7.2}B_{0.8}$

An SEM picture of the surface of a sample, that had been polished and etched, is shown in Fig 5.7. The grains observed appear to be white, approximately 1-2 μm in size. From EDXA, the grains and the grey colored boundary appear to have an atomic composition of, approximately, $Fe_{85}(NdDy)_{15}$. This composition of atoms, possibly, corresponds to $Fe_{14}(NdDy)_2(CB)_1$. The dark

phase shows a composition of approximately 50 at% Fe and 50 at% Nd and Dy. This could, possibly, be the $Fe-(NdDy)-(CB)$ phase. Fig 5.8-9 show the microstructure and the corresponding diffraction pattern. The 2:14:1 phase is the one responsible for this pattern. The distortion, appearing as a curvature at the edges, in the pattern is due to the presence of faults in the sample. Lattice imaging, Fig 5.10, gives a "d" spacing of about 1.82 nm. The diffraction pattern for this lattice, Fig 5.11, is possibly a hexagonal structure with a = 9.3 nm and two different c-distances corresponding to, approximately c = 8 nm and c = 18 nm. This structure is possibly the Fe-Dy-C phase with stacking faults, [15]. Fig 5.12 shows grains which appear to be oriented. The smallest grain is about $0.25\mu m$ long. The other grains, parts of which we observe, are probably larger than $0.25\mu m$.

Note that the 2:14:1 phase is not formed with Fe, Nd and C as the metalloid, [21]. X-ray observations showed that the bulk phase is the 2:14:1 phase.

5.4 Microstructure of $Fe_{76.1}Nd_{10.1}Dy_{5.9}C_{7.1}B_{0.8}$

SEM, Fig 5.13, shows small white grains embedded in a dark phase. EDXA of the small grains shows that it has an at% composition of $Fe_{85}Nd_9Dy_6$. It is possible that this phase corresponds to $Fe_{14}(NdDy)_2(CB)_1$. The second phase contains approximately, $Fe_{81}Nd_{11}Dy_8$. The grains are, approximately 1-3 μm in size.

Domain walls are observed ,as shown in Fig 5.14, and the diffraction pattern

shows the presence of the rhombohedral Fe_2Dy_{17}, called 2:17 for convenience, phase, as in Fig 5.15 . The indexing for the 2:17 phase was done by using the data for Sm_2Co_{17} with a = 8.38×10nm and c = 12.63×10nm. Fig 5.16 shows the microstructure of some region of the sample. We observe that the diffraction pattern from the region labelled X, as shown in Fig 5.17, is identified as the 2:14:1 phase. The "d" spacing from the lattice image of Fig 5.18 is calculated to be about 15 × 10nm. The diffraction pattern from this area of the sample gives us the $Fe - Dy - C$ phase and is shown in Fig 5.19 (compare with Fig 5.10).

As before, X-ray diffraction was done and they are consistent with the electron diffraction, and the 2:14:1 phase is seen along with the 2:17 phase. One of the lines which is strongly intense, could possibly correspond to the Fe_2DyC_2, [15], phase.

5.5 Microstructure of $Fe_{77}Nd_{15}B_8$

Fig 5.20 is an SEM picture of the not heat-treated sample which shows long plate-like grains. The white contrast is provided by another phase which could be the Nd-rich phase or a mixture of the Nd-rich phase and Nd_2O_3,tentatively called FeNdB. In fact, what we see is the grain boundary along which the FeNdB phase exists. The grains are about 20-30 μm in size. The SEM for the as-cast sample that had been heat-treated , called IV for convenience, shows a similar microstructure as the not heat-treated sample, Fig 5.21. But now the grains appear to be bigger than 30μm, and the FeNdB phase is also observed.

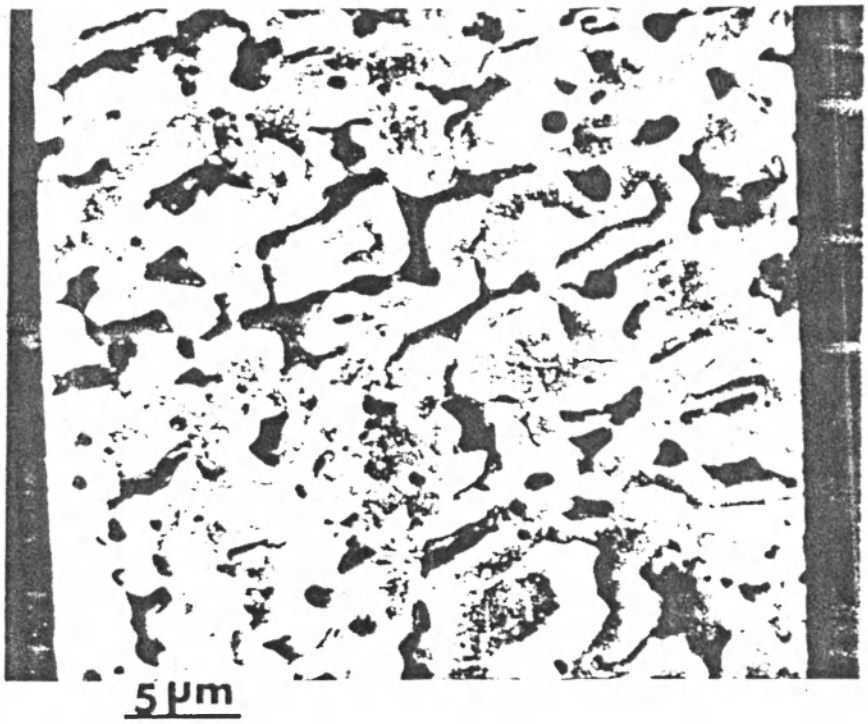

Fig 5.1 SEM of I showing three different grains

Fig 5.2 Microstructure of a region of I

Fig 5.3 Electron diffraction pattern of region A in Fig 5.1 showing the $Fe_{14}Dy_2C$ phase.

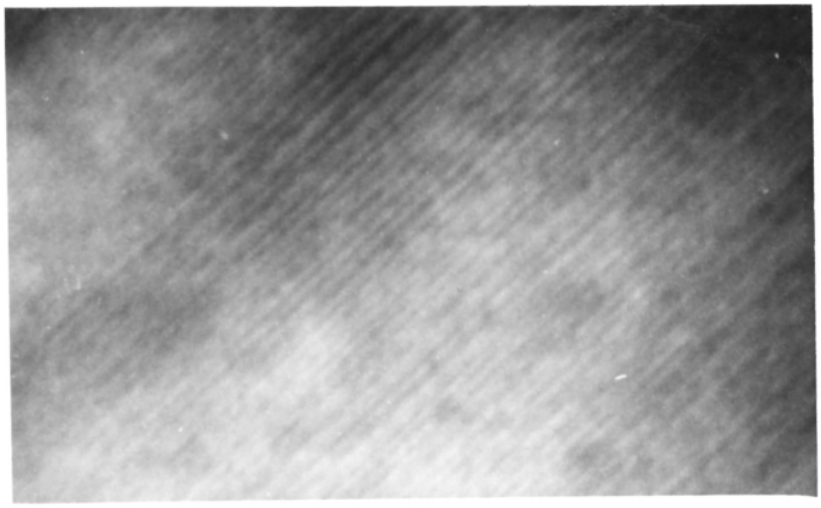

Fig 5.4 Lattice image of the 2:14:1 phase

Fig 5.5 Microstructure of a diffrent region of I

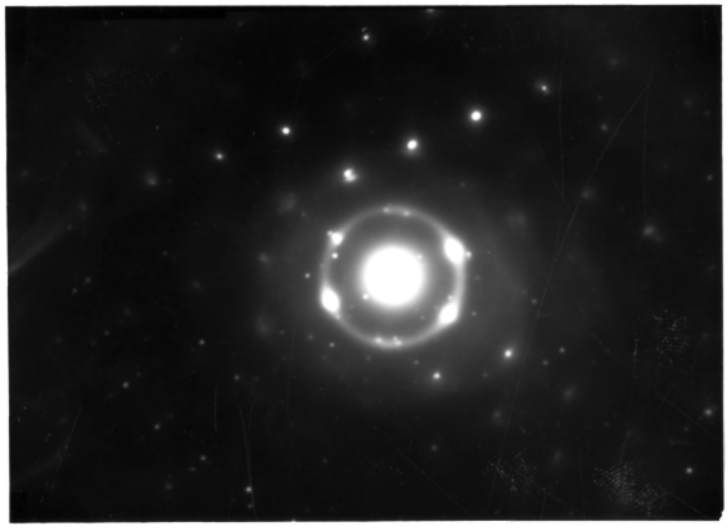

Fig 5.6 Electron diffraction of region in Fig 5.5

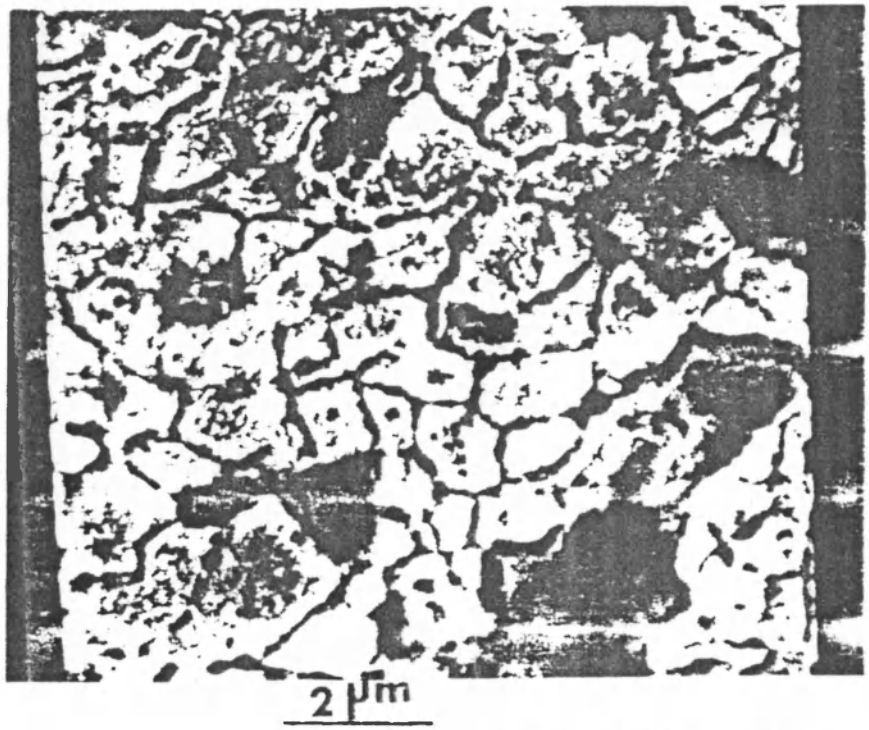

Fig 5.7 [illegible] of II showing grains 1-2μm in size

Fig 5.8 Microstucture of a region of II

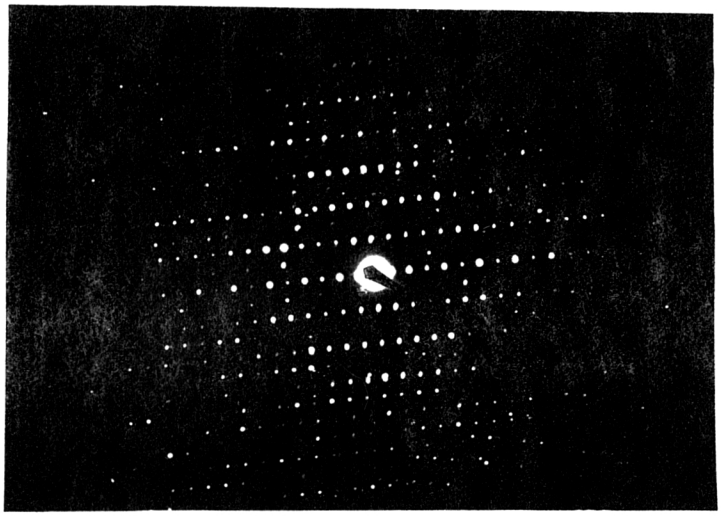

Fig 5.9 Electron diffraction pattern of 2:14:1 phase showing faults

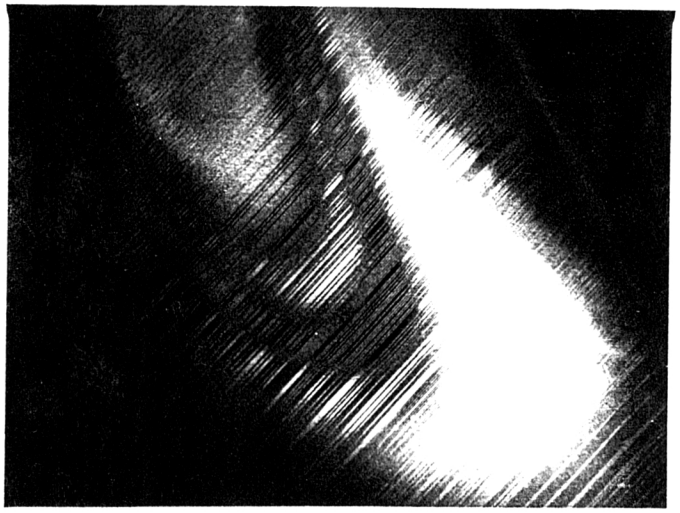

Fig 5.10 Lattice images seen in II

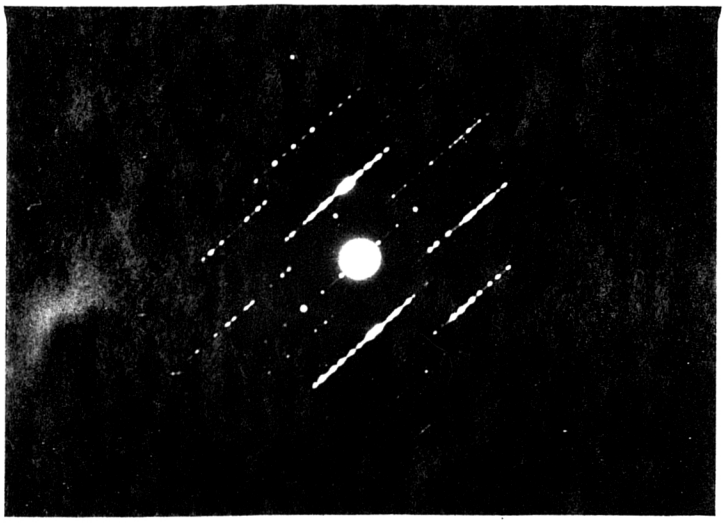

Fig 5.11 Electron diffraction pattern of Fig 5.11 showing hexagonal structure

Fig 5.12 Microstructure of II showing oriented grains

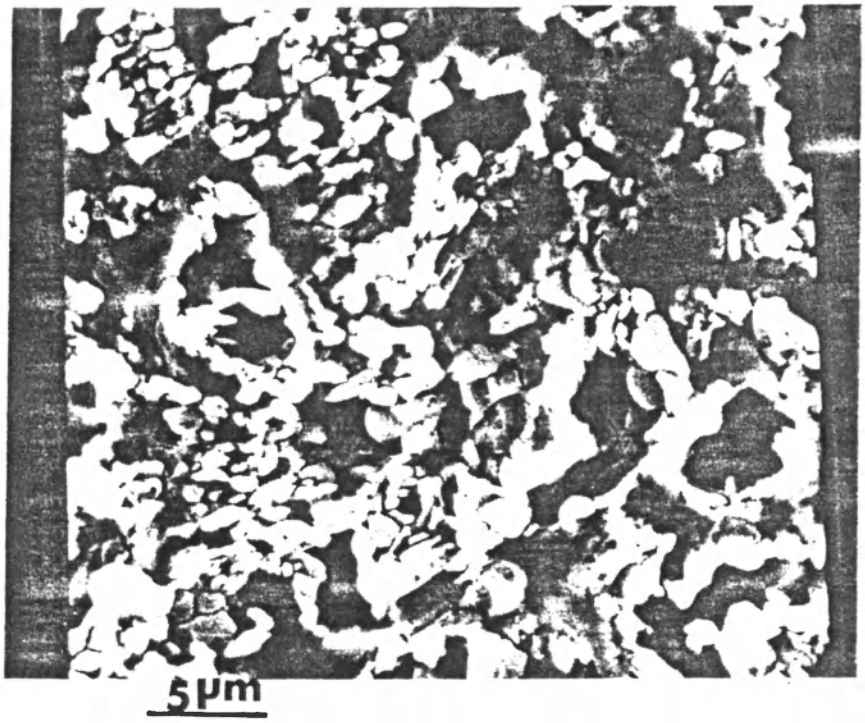

Fig 5.13 SEM of III

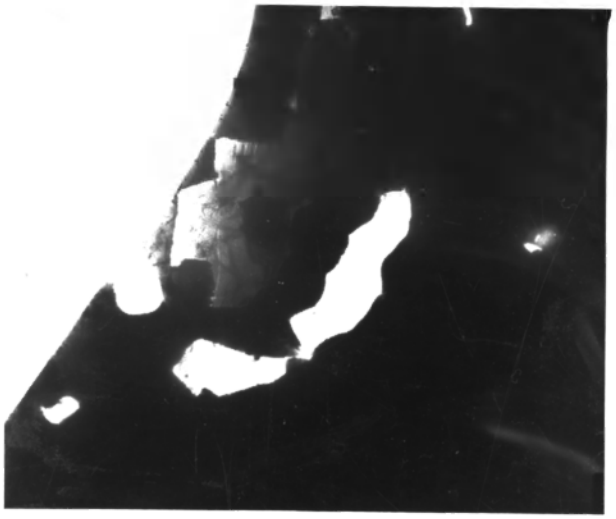

Fig 5.14 Domain wallsdw in III

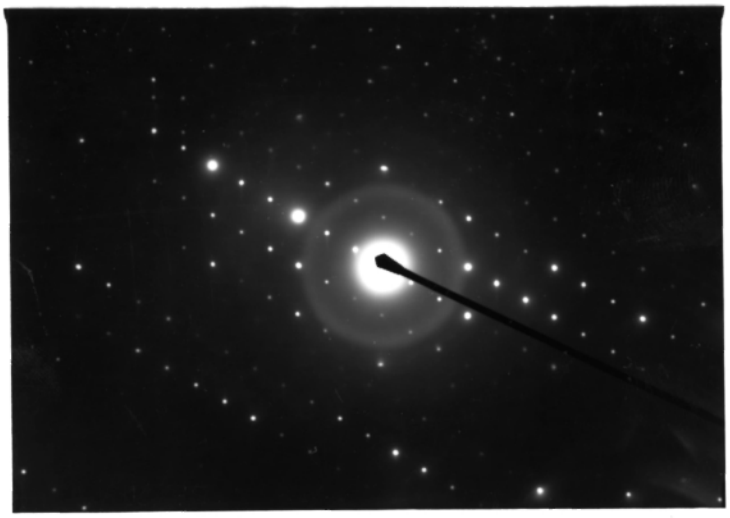

Fig 5.15 2:17 phase corresponding to the dw of Fig 5.14

Fig 5.16 Microstructure of some region of III

Fig 5.17 2:14:1 phase corresponding to region X

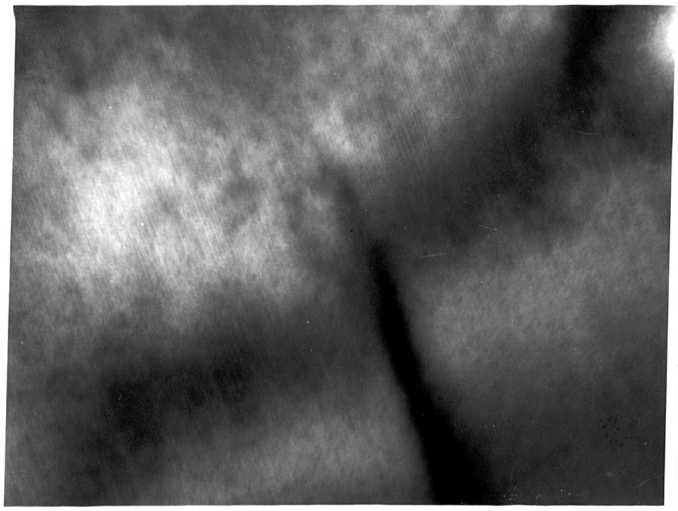

Fig 5.18 Lattice image of another region of III

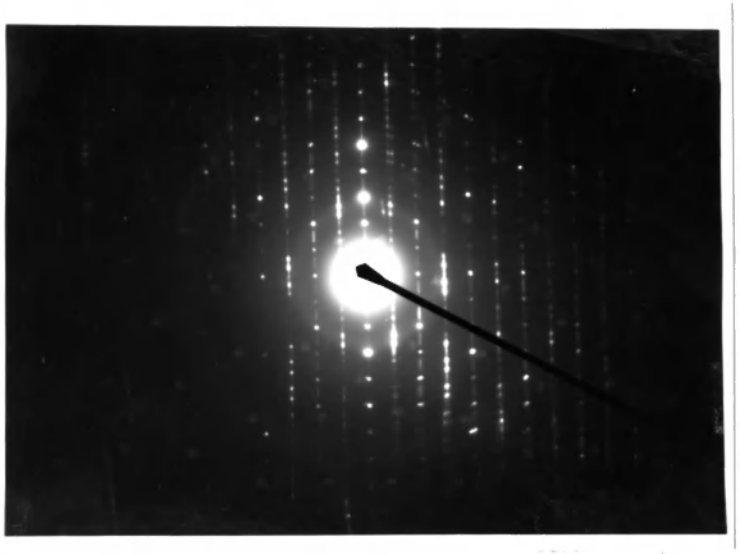

Fig 5.19 FeDyC phase corresponding to the lattice image of fig 5.18

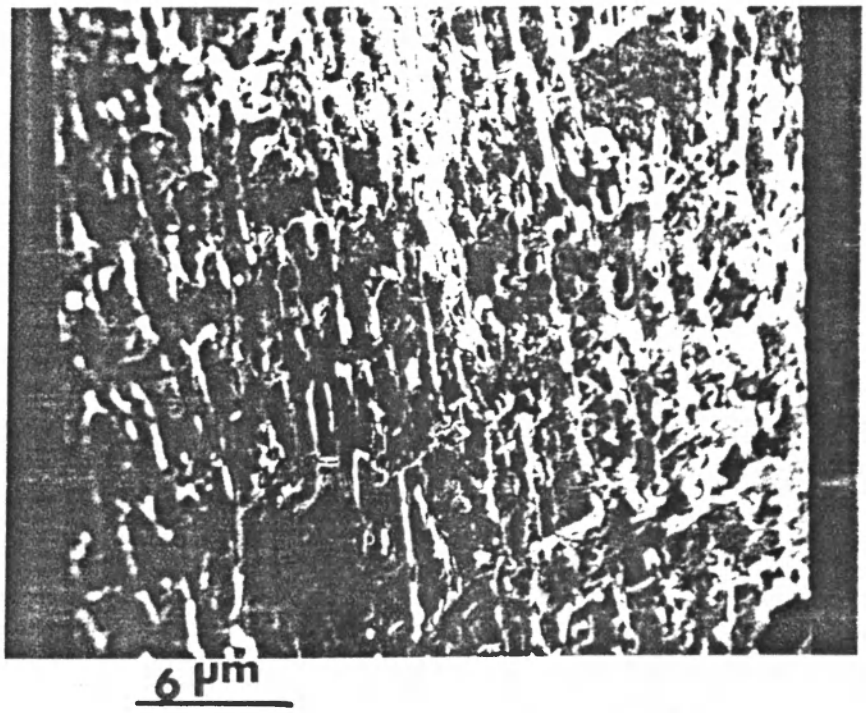

Fig 5.20 SEM of as cast $Fe_{77}Nd_{15}B_8$

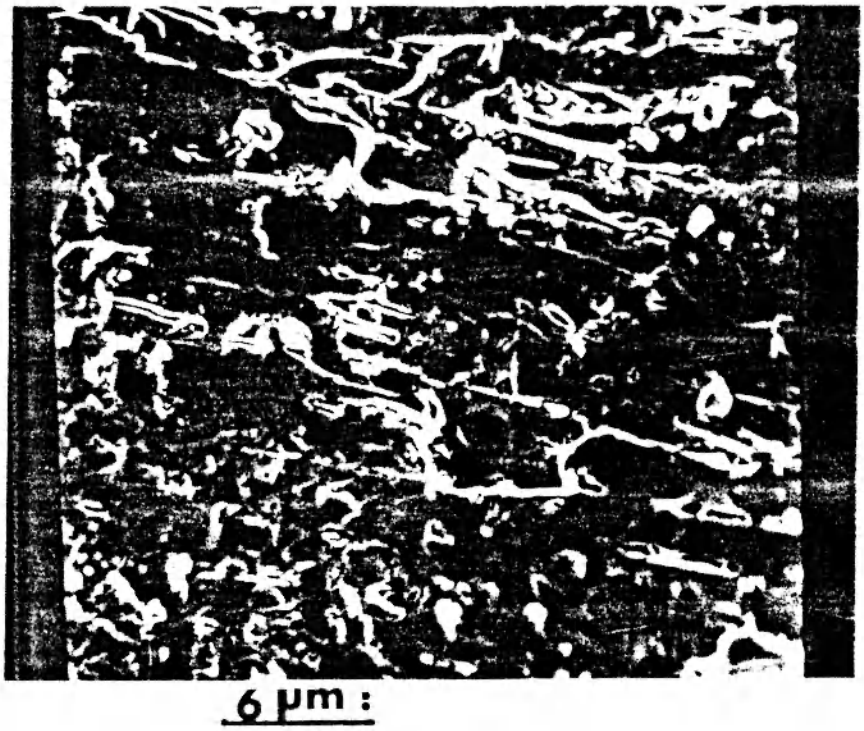

Fig 5.21 SEM of as cast heat treated $Fe_{77}Nd_{15}B_8$

Chapter 6

ANALYSIS AND CONCLUSIONS

6.1 Phase Diagram

The objective of this chapter, is to put together the data and microstructure presented in the previous chapters and then come up with an explanation for the existence of large coercivity in as-cast Fe-R-C-B at room temperature.

The as-cast alloys that were not heat-treated did not show any coercivity at room temperature. The as-cast material, after solidification has the rhombohedral $Fe_{17}Dy_2$ which is soft and H_C is very small. This phase is transformed to the magnetically hard $Fe_{14}Dy_2C_1$ upon annealing at 900°C [8]. Now there are two mechanisms by which one could obtain the 2:14:1 phase. (i) transformation from α-Fe [23], by heat treatment or (ii) transformation from $Fe_{17}R_2$ or a derivative of it [8], by heat treatment.

Let us consider the ternary phase diagram corresponding to I. From [8], we know that the $Fe_{14}Dy_2C_1$ phase can be formed from the following mechanisms:

(i). $Fe_{17}R_2$ + Fe-R-X = $Fe_{14}R_2X_1$ + R-rich Phase

(ii). $Fe_{17}R_2X$ + Fe-R-X = $Fe_{14}R_2X_1$ + $Fe_2R_1X_2$

Where R = Dy, Nd and X = C, C_xB_{1-x}

Therefore when microstructure determinations are made a search for the above phases should be made. The choice of 900°C as the annealing temperature

is explained by the phase diagram. At this temperature, for the composition of I, ie., $Fe_{77}R_{15}C_8$, the three phases $Fe_{17}R_2$, $Fe_{14}R_2C_1$, and FeRC are in equilibrium[8]. Therefore it is reasonable to expect a transformation around this temperature. The long annealing time of 72 hours was chosen as being appropriate to allow for the optimum transformation of the 2:17 phase to the 2:14:1 phase.

6.2 Magnetic Hardening

The microstructure studies of I, II, and III show the presence of more than one phase.The magnetically hard phase has been identified as $Fe_{14}Dy_2C$. M vs T data predicts a T_c of approximately 300°C which agrees nicely with the reported value of 280° [18].The same data confirms the presence of a multiphase microstructure, which agrees with the SEM's, the metallurgy data and the TEM. It is likely that the anomalies observed in Ac susceptibility data at around 175 K is due to spin reorientation. It can be concluded large grains of $Fe_{14}Dy_2C$ and irregularly distributed smaller grains of $Fe_{17}Dy_2$ and some other phase, tentatively called Fe-R-X phase.

It is likely that the high coercivity we have observed in these samples is due to the formation of single domain particles. To check this we calculated the single domain particle size, using the relation $D_c = \frac{1.4\gamma}{M_s^2}$, [25]. From (1.4) and (1.3), using $J_e = 0.3kT_c$, [24], assuming a high value of K = 10^8 ergs/cc , a = 9°A, we get $\gamma = 15.85 ergs/cm^2$. Note that for $Fe_{14}Nd_2B$ K = 4×10^7

ergs/cc and it is known that K increases for Dy. Therefore, it was justified to use the K value given above. Since the density of the samples were not known, M_s in emu/cc was obtained by assuming a density of 8 gm/cc. So we have for I, $M_s = 8g/cc \times 30emu/g = 240emu/cc$, where 30 emu/g is an approximate value for M_s, from table 4.1. Using the above we get $D_c = 4.4\mu m$. Since M_s for II and III are greater than the M_s value for I, therefore they have a lower D_c value. So it is safe to conclude that, assuming high reliability of the relation for D_c, the single domain particles have a size whose upper limit is $4.4\mu m$.

As the grain sizes found from microstructure studies are 1-3 μm, except for I, it is likely that the coercivity of our samples, II and III is due to formation of single domain particles. This result is, of course under the tacit assumption that $D_c = \frac{1.4\gamma}{M_s^2}$, is a reliable relation. The coercivity predicted by noninteracting SDP's is $H_c = \frac{K}{M_s}$, which calculates to about 40 kOe. This value is much higher than the expected value of about 15 kOe. However, the high values of $\frac{M_r}{M_s}$, about 0.7, point to a strong interaction between domains. The SEM's show us grains of 2:14:1 which are essentially contiguous with Fe-R-X dispersed at random. So it is possible that there is an interaction between these domains. As for I, the grains are much greater than D_C therefore we can declare with confidence that the H_C for I is not due to SDP's. In all of the samples, we identified the 2:14:1 phase and the microstructure did not show any pinning sites. The initial curves, Figs 4.1-3, show that there are no pinning sites inside the grains. Therefore, the magnetization reversal has to occur at the grain boundaries otherwise one

reverse domain could give rise to magnetization reversal of the whole magnet. The phase at the grain boundary is most probably the Fe-R-X phase. Therefore the nucleation of reversed domains occurs at this phase. This mechanism, is most likely, the one responsibl e for magnetization reversal. The argument that reversal occurs due to rotation of SDP has it's strengths but we are not sure of the calculated value for D_C.

6.3 Effect of C on coercivity

Comparing the SEM's of I, II, III, and IV we can find out the effect of C on the coercivity. Magnetic measurements for IV did not show any coercivity, Fig 6.1 . In all of these the 2:14:1 phase was present. However, in I, II, and III the size of the 2:14:1 grains were much smaller than in IV. This is consistent with the observed increase in H_c with decreasing particle size [2]. The extreme case occurs in ribbons where the grain size is approximately 400°A [26]. So we can conclude that C aids in the formation of small grains.

6.4 Effect of Nd on coercivity

It is well known that Fe and Nd couple ferromagnetically. Therefore addition of Nd increases the magnetization and hence $(BH)_{max}$ can be increased. But coercivity depends on the structure of the phase and the high anisotropy of the 2:14:1 phase helps increase H_c. Fig 6.2 shows that IV has a negligible coercivity. The reason is that upon substitution of Dy with Nd the anisotropy

field is decreased. Also the grains are much larger than the grains formed by alloys with C as the metalloid.

6.5 Effect of Dy on the coercivity

I, II, and III show large coercivities and this has been shown to be due to the formation of SDP's of the $Fe_{14}Dy_2C_1$ phase which is formed when the as-cast alloy is annealed. To check whether H_C could be due to the anisotropy introduced by Dy, we measured the H_c for $Fe_{77}Dy_{15}B_8$, both as-cast and as-cast heat-treated. We find that the coercivity in both cases is close to 2 kOe. This means that the anisotropy of Dy does not play a major role in the experimentally observed large coercivities.

Fe and Dy couple anti-ferromagnetically and this reduces the magnetization and therefore the energy product. By adding Nd we can increase M, but now we need to add a little B to stabilize the hard magnetic phase. This is because now lesser number of s, p electrons are needed to stabilize the structure. It is to be noted that the 2:14:1 phase is composed entirely of C, as is expected statistically.

6.6 Conclusions

1. The outstanding magnetic properties of Fe-R-C alloys can be attributed to the $Fe_{14}Dy_2C_1$ phase.

2. The $Fe_{14}Dy_2C_1$ has the following properties, [20], :

i) a = 0.8756 nm and c = 1.1801 nm

ii) $T_c = 553K$

iii) Easy axis is along the "c" axis.

3. Unlike Fe-Nd-B alloys, the 2:14:1 phase does not crystallize out of the melt. This means that it is possible to increase H_c by metallurgical manipulation , for example, by introducing pinning sites etc which could hinder, the rotation of the SDP during magnetization reversal, or the movement of domain walls.

4. Unlike Fe-Nd-B alloys does not require special processing such as powder metallurgy, rapid solidification etc. In Fe-R-C alloys the 2:14:1 phase is developed upon heat treatment of the as-cast alloy.

5. The grains formed by using C as the primary metalloid are small as compared to the grains formed by using B.

6. Magnetization reversal in these alloys takes place via the incoherent rotation of SDP's in II and III, or due to nucleation of reversed domains in all the samples. The latter is more likely.

7. The Fe-Dy-C alloys have a low magnetization and it can be improved by proper addition of Nd and a bit of B to stabilize the 2:14:1 phase. Another serious disadvantage of the Fe-R-C magnets is their low T_c.

8. The microstructure of these alloys shows the presence of the 2:14:1, the 2:17, the Dy-rich, the Dy-oxide phases and the Fe-R-X phase.

9. All of the samples studied, showed grains which had no preferred orientation . It would be beneficial to orient the magnet during as-cast solidification. Then, when the sample is heat-treated the primary phase transforms to the 2:14:1

phase in the same conFiguration and we obtain grains which are all oriented in the same direction. In such a case we would expect the H_c to increase.

REFERENCES

1. "Principles of Ferromagnetic Behaviour", W.J.Carr Jr., from "Magnetism & Metallurgy" , Vol 1, edited by Berkowitz & Kneller, Academic Press 1969.

2. "The Physical Principles Of Magnetism" , Allan H.Morrish, John Wiley & Sons, Inc., 1965.

3. "Magnetism & Metallurgy Of Soft Magnetic Materials" , C.W.Chen, from "Selected Topics In Solid State Physics" , Vol 15, edited by E.P.Wohlfarth, North-Holland Publishing Company, 1977.

4. Brown Jr.,W.F., 1957, Phys. Rev. 105, 1479

5. "Magnetic Materials and their Applications" , Heck I.C. , Crane, Russak & Company Inc., 1974.

6. "Ferromagnetic Materials" , Vol 3, Edited by E.P.Wohlfarth, North-Holland Publishing Company, 1982, p. 44.

7. N.C.Liu & H.H.Stadelmaier, Mater.Lett, 4, 377 (1986)

8. "High intrinsic coercivities in iron-rare earth-carbon-boron alloys through the carbide or boro-carbide $Fe_{14}R_2X(X = B_xC_{1-x})$", Liu N.C., Stadelmaier H.H. & Schneider G (to be published).

9. G.C.Hadjipanayis, R.C.Hazelton, & K.R.Lawless , J. Appl. phys. **55** (6), 2073(1984).

10. G.C. Hadjipanayis, R.C.Hazelton, & K.R.Lawless, Appl. Phys. Lett. **43**, 797(1983).

11. J.J.Croat, J.F.Herbst, R.W.Lee, & F.E.Pinkerton, J. Appl. Phys. 55(6), 2078(1984).

12. N.C.Koon & B.N.Das, J. Appl. Phys. 55(6), 2063(1984).

13. Sumitomo Special Metals Co. Ltd. , Osaka, Japan

14. M.Sagawa, S.Hirosawa, H.Yamamoto, S.Fujimura, & Y.Matsuura, Jap. J .Appl .Phys. 26(6), 785(1987).

15. H.H.Stadelmaier & H.K.Park, Z.Metallkunde72, 417(1981).

16. J.Schneider, A.Handstein, R.Grossinger, & S.Heisz, Proc. of third intl.conf., Physics of Magnetic Materials, Sept.1986, p.225 17. K.-D.Durst & H.Kronmuller, J. Magn. Magn. Mat. 68 , 63(1987).

18. A.T.Pedziwiatr, W.E.wallace, and E.Burzo, J. Magn. Magn. Mat. 59, L179 (1986).

19. J.W.Edington, Practical Electron Microscopy in Materials Science Mono. 2 , Electron Diffraction in the Electron Microscope, Macmillan, 1975.

20. M.Brilonizhka & Yu. B, Inorg. Matls 10 (1974).

21. R.van MENS, J. Magn. Magn. Mat. 61, 24 (1986).

23. H.H.Stadelmaier, N.C.Liu, and N.A. El Masry, Mater. Lett. 3, 130 (1985).

24. B.D.Cullity, Introduction to Magnetic Materials, Addison-Wesley Publishing Co., 1972.

25. Livingston, J. App. Phys. **57**, 4137 (1985).

26. G.C.Hadjipanayis, and Gong Wei, J. Magn. Magn. Mat. **66**, 390 (1987).

27. Yi Fei Tao, Ph.D thesis, Dept. Physics, Kansas St. Univ., 1986.

28. J.F.Herbst, J.J.Croat, F.E.Pinkerton, and W.B.Yelon, Phys Rev B, **29**, 4176 (1986).

29. D.Givord, H.S.Li, and J.M.Moreau, Solid State Commun. **50**, 497 (1984).

30. "Ferromagnetic Materials", Vol 1, Edited by E.P.Wohlfarth, North Holland Publishing Company, 1980, p. 388.

MAGNETIC AND MICROSTRUCTURE PROPERTIES OF IRON-RARE EARTH-CARBON MAGNETS

by

N. VENKATESWARAN

B.E., B.I.T.S. Pilani, India, 1985

AN ABSTRACT OF A THESIS

submitted in partial fulfillment of the

requirements for the degree

MASTER OF SCIENCE

Department of Physics

College of Arts and Sciences

KANSAS STATE UNIVERSITY

Manhattan, Kansas

1988

ABSTRACT

The new generation of cobalt free Fe-Nd-B magnets have excellent hard magnetic properties which are attributed to the tetragonal $Fe_{14}Nd_2B$ phase that has a high anisotropy and magnetic moment. Substitution of B with C and Nd with Dy leads to a substantial increase in coercivity and a drop in magnetization in as cast samples. The purpose of this work has been to study the magnetic and microstructure properties of Fe-R-C based systems. The magnets used were heat-treated as-cast samples. The outstanding hard magnetic properties of this system has been attributed to the $Fe_{14}Dy_2C$ phase that has a higher anisotropy but a lower magnetic moment as compared to $Fe_{14}Nd_2B$. The substitution of Nd and B for Dy and C enhances the magnetic moment of Fe-Dy-C, but reduces the coercivity significantly. The origin of high coercivity has been examined by correlating the hard magnetic properties with the microstructure. The high coercivity and the magnetization reversal can be explained by both the nucleation of reversed domains and interacting single domain particles respectively.